In high grade ovarian carcinoma, platinum-sensitive tumor recurrence and acquired-resistance derive from quiescent residual cancer cells that overexpress CRYAB, CEACAM6 and SOX2

Stanislas Du Manoir, Hélène Delpech, Béatrice Orsetti, William Jacot, Nelly Pirot, Jean Noel, Pierre-Emmanuel Colombo, Claude Sardet, Pierre-emmanuel Colombo, Charles Theillet

HAL Id: inserm-03613881
https://inserm.hal.science/inserm-03613881

Submitted on 18 Mar 2022

High Grade Ovarian Carcinoma Platinum-sensitive tumor recurrence and acquired-resistance derive from quiescent residual cancer cells that overexpress CRYAB, CEACAM6, SOX2

doi.org/10.1002/path.5896

Stanislas du Manoir[1&], Hélène Delpech[1], Béatrice Orsetti[1], William Jacot[1], Nelly Pirot[1], Jean Noel[3], Pierre-Emmanuel Colombo[1], Claude Sardet[2], Charles Theillet[1&].

[1]IRCM U1194, INSERM, Univ Montpellier, ICM, 208, rue des Apothicaires, F-34298 Montpellier, Cedex 5, France Montpellier, France.

[2]IRCM U1194, INSERM, Univ Montpellier, ICM, CNRS, Montpellier, France.

[3]BCM, Univ. Montpellier, CNRS, INSERM, Montpellier, France.

[&]corresponding authors: stanislas.dumanoir@inserm.fr; charles.theillet@inserm.fr

The authors declare no potential conflicts of interest

Abstract

Most High-Grade Ovarian Carcinomas (HGOCs) are sensitive to carboplatin (CBP)-based chemotherapy but frequently recur within 24 months. Recurrent tumors remain CBP-sensitive and acquire resistance only after several treatment rounds. Recurrences arise from a small number of residual tumor cells hardly amenable to investigation in patients. We developed Patient-Derived Xenografts (PDXs) that allow the study of these different stages of CBP-sensitive recurrence and acquisition of resistance.

We generated PDX models from CBP-sensitive and intrinsically resistant HGOC. PDXs were CBP- or mock-treated and tumors were sampled, after treatment and at recurrence. We also isolated models with acquired-resistance from CBP-sensitive PDXs. All tumors were characterized at the histological and transcriptome levels.

PDX models reproduced treatment response seen in the patients. CBP-sensitive residual tumors contained non-proliferating tumor cells clusters embedded in a fibrotic mesh. In non-treated PDX tumors and treated CBP-resistant tumors fibrotic tissue was not prevalent. Residual tumors had marked differences in gene expression when compared to naïve and recurrent tumors, indicating downregulation of cell cycle and proliferation and upregulation of interferon response and epithelial–mesenchymal transition. This gene expression pattern resembled that described in embryonal diapause and 'drug-tolerant persister' states. Residual and acquired-resistance tumors share the overexpression of three genes – *CEACAM6*, *CRYAB*, and *SOX2*.

In HGOC PDX, CBP-sensitive recurrences arise from a small population of quiescent, drug-tolerant, residual cells embedded in a fibrotic mesh. These cells overexpress *CEACAM6, CRYAB* and *SOX2*, a signature also associated with acquired resistance and poor patient prognosis, which, thus, might serve as a biomarker to predict recurrence and emergence of resistant disease in CBP-treated HGOC patients.

Introduction

High-Grade Ovarian Cancer (HGOC) is commonly diagnosed at advanced stages, once the tumor has disseminated in the abdominal cavity. Standard therapy involves surgical debulking and chemotherapy, but for the past two decades the 5-year HGOC survival rate has not exceeded 30% [1]. The standard chemotherapy is based on a combination of carboplatin (CBP) and paclitaxel, in which platinum is the determining component. The majority of patients with CBP-sensitive disease will recur within 6–24 months leading to a clinical classification based on the interval between the last cycle of chemotherapy and the first recurrence or platinum-free interval (PFI) [2]. Moreover, there is a strong association between incomplete debulking and early recurrence, highlighting the importance of residual tumor volume in HGOC relapse [3].

Surprisingly, platinum-sensitive HGOC recurrence remain sensitive to CBP. Patients may undergo several cycles of treatment before the tumor ceases to respond or the accumulated toxicity precludes further chemotherapy [4]. The mechanism(s) underlying these CBP-sensitive recurrences remain obscure and a Darwinian selection of a genetically distinct subset of platinum-resistant cells is an insufficient explanation [5]. Residual tumor cells surviving treatment may act as the seeds of recurrence, however, their nature in HGOC have been poorly documented. To our knowledge, the mechanisms underlying their persistence after treatment have been investigated only in ovarian cancer cell lines in culture [6]. Several mechanisms have been proposed to explain transitory resistance of residual cancer cells after treatment. These include presence of persistent drug tolerant cells, possibly bearing cancer stem cell (CSC) properties and impaired apoptosis [7],[8],[9], as well as a transitory modification of the stromal environment limiting the penetration of chemotherapeutic agent [4],[10].

The availability of residual tumor tissue from HGOC patients for study is limited because second surgery after chemotherapy is not commonly performed [2]. To investigate the nature of residual cells after CBP treatment, in this study we used patient-derived xenografts (PDXs) of HGOC grafted onto immunocompromised mice as a model system allowing to sample tumors prior to treatment (naïve), after treatment (residual), upon regrowth (recurrent) and upon acquisition of resistance (acquired-resistant). We show that these PDX models accurately recapitulate the clinical features of the original patient tumors. Post-treatment residual tumors contain small clusters of non-proliferating tumor cells embedded in fibrotic

tissue. The transcriptomes of the residual tumors after treatment are distinct from naive and recurrent tumors. Their gene expression resembles that seen in embryonal diapause, which has been associated with the 'drug-tolerant-persister' phenotype [11],[12]. Genes involved in cell cycle and proliferation are strongly down-regulated, whereas genes involved in inflammation, the interferon response and the epithelial–mesenchymal transition (EMT) are up-regulated. Notably, three genes –*CEACAM6, CRYAB* and *SOX2* – are overexpressed in both residual tumors and tumors that acquired resistance to CBP. Our findings suggest that recurrent CBP-sensitive HOGC arises from a small population of transiently quiescent, residual tumor cells embedded in a dense fibrotic mass, which are able to evade the effects of chemotherapy drugs. Overexpression of *CEACAM6, CRYAB* and *SOX2* may prove useful as a biomarker to predict recurrence and emergence of CBP-resistant HGOC.

Materials and Methods

Patient tumor provenance and ethics statement

The study was approved by the ethics committees for animal experimentations of the University of Montpellier (CEEA-LR-12028). Human ovarian tumors were obtained from the Biobank BB033-00059 initiated by Pr. P-E Colombo (ICM, Montpellier) under the management of the CRB-ICM (biological resource center) of the Montpellier Cancer Institute (ICM), Grant ICM-CORT-2020-20 project IHC-HGOC.

HGOC PDX models and in vivo treatment

Ovarian cancer PDX model establishment has been previously described [13].

Initial treatment: PDX of about 100-150mm3 were treated by a cycle of CBP (4 weeks, 50mg/kg CBP, twice/week) or vehicle for as seen in Fig. 1A. Monitoring of relapse: After complete regression of sensitive PDXs, relapses were monitored for up to 9 months. *In vivo* acquisition of resistance: In case of relapse, additional CBP cycle(s) were administered upon no regression was observed under treatment (Fig. 4). Further details on *in vivo* experiments are described in the Supplementary information.

RNA extraction and transcriptome analysis

RNAs were extracted from frozen tumor fragments collected after one month (one cycle of CBP or mock-treated) and after acquisition of resistance using RNeasy Mini Kit (Qiagen, Les Ulis, France). Expression profiling was performed on Affymetrix Human Genome GeneChip U133Plus2 at the MGX-transcriptome platform (BioCampus-IRMB) according to the manufacturer's recommendation. Differentially expressed genes between residual tumor (one cycle of CBP versus mock-treated) or between in vivo acquired resistant and untreated tumors using Rankproduct algorithm. Data analysis is detailed in the Supplementary information.

Exome sequencing and analysis of BRCA1 methylation status from untreated PDXs was done.

(See Supplemental information)

Histological analysis

Experimental procedures used for immunohistochemical staining and quantification (Picro-Sirius Red…) and antibodies used for IHC (against Ki-67, caspase, PAX8, CRYAB, CEACAM6, SOX2) are detailed in the Supplementary information.

Results

Patient-derived xenografts of high-grade ovarian cancer recapitulate the clinical response to carboplatin

To investigate the mechanisms of regression, recurrence and acquired resistance to carboplatin (CBP) in HGOC, we used 10 PDX models selected from our collection of HGOC PDXs [13], according to the recorded time to recurrence in the patients (Table 1). We selected tumors: (i) refractory or intrinsically resistant to treatment (progression under treatment or recurrence within 6 months), (ii) sensitive disease (recurrence after 12 months). Four models, designated hereafter CBP-resistant (PDXs O3053, O2815, O3111, O3264, recurrence free survival or RFS 0-230 days), corresponded to resistant disease. Six other models, designated CBP-sensitive tumors (PDXs O3312, O8378, O7876, O5588, O1047, O4571; RFS 353–4335 days), were derived from sensitive tumors (Table 1, Figure 1A). The 10 PDX models were analyzed by whole exome sequencing for DNA mutations and by methyl-specific PCR (MS-PCR) hypermethylation of the BRCA1 promoter. Four of the six CBP-sensitive models presented *BRCA1*-deficiency (2 coding pathogenic *BRCA1* mutations and 2 hypermethylation of the *BRCA1* promoter). The ten PDX models were derived from FIGO stage IIIC or IV tumors (Table S1).

PDX models were grafted on Swiss/Nude mice to monitor their response to CBP. Mice were injected intra-peritoneally (IP) twice a week for 4 weeks with 50 mg/kg of CBP or the vehicle solution. PDXs derived from CBP-resistant tumors showed little response to CBP: tumor volumes were stable or grew under treatment (Figure 1A). Contrastingly, CBP-sensitive PDXs showed a complete macroscopic regression within 6 weeks after the start of treatment (Figure 1A and Figure S1). Some of the CBP-sensitive PDX regressed rapidly (twofold volume reduction within 14 days of treatment, blue lines) whereas others regressed more slowly (green lines). The mice were surveyed for tumor recurrence for up to 9 months after the end of treatment. CBP-sensitive tumors started to regrow at the same anatomical location after 30–230 days (Figure 1B). PDXs that regressed most rapidly upon CBP-treatment (blue lines) regrew later than those that regressed more slowly (green lines).

PDX response to CBP and interval to tumor regrowth were in accordance with the clinical history of the patients from which the PDX models originated (Table 1, Figure 1A-B, Table S1). In particular, O1047 and O4571 took at least 100 days to relapse in mice and originated

from tumors showing the longest RFS (over 8 years) compared with other tumors whose RFS ranged 11 to 22 months.

We assessed cell proliferation of CBP-resistant and CBP-sensitive PDX tumors at the end of treatment by Ki-67 immuno-staining and found striking differences.

Percentage of Ki-67-positive cells were strongly reduced in residual tumors of treated CBP-sensitive PDX compared with mock-treated controls (paired t-test, p=0.009, Figure 1C and Figure S2). This reduction was stronger in fast-regressing tumors. Contrastingly, percentage of Ki-67-positive cells were increased in treated versus control CBP-resistant PDX tumors (paired t-test, p=0.0095) (Figure 1C, Figure S2). Staining for the cell death marker caspase-3 showed no difference between CBP and mock-treated PDX: all tumors from both CBP-sensitive and CBP-resistant PDX models – including residual tumors – contained about 1% caspase-3-positive cells (Figure S3). Together, these data indicate that most cancer cells in CBP-sensitive residual tumors have stopped proliferating and are negative for cell death markers, features consistent with a viable and quiescent state.

Residual tumor cells in treated CBP-sensitive tumors are embedded in a fibrotic mesh

Because surgery is not a common practice after CBP chemotherapy for HGOC, analysis of residual tumor tissue from patients is little documented. Our PDX models provide the opportunity to perform detailed histological and molecular characterization of HGOC during and after treatment.

As demonstrated by PAX8 immunostaining (a marker of human ovarian carcinoma cells [14]) treated CBP-sensitive tumors contained few residual human ovarian carcinoma cells organized in small dispersed clusters embedded in a dense stroma (Figure 2A). Staining with Picro-Sirius Red revealed that this dense stroma was composed of fibrotic tissue encompassing most of the tissue section. No extensive fibrosis was observed in mock-treated CBP-sensitive models. Contrastingly, in treated CBP-resistant PDX, Red Sirius staining areas were restricted to the periphery of the tumor and treated samples did not show increased fibrosis (Figure 2B, Figure S4).

These data indicate that CBP treatment of sensitive HGOC results in a rapid reduction of the bulk of the tumor concomitant with a massive build-up of a dense fibrotic network containing small clusters of non-proliferating, residual PAX8-positive tumor cells.

Residual CBP-sensitive tumors have gene expression profiles indicative of proliferation downregulation and upregulation of inflammation and Epithelial-Mesenchymal Transition

We hypothesized that the residual cells embedded in the dense fibrotic mesh in CBP-treated tumors might show gene expression profiles reflecting signaling pathways contributing to response to treatment and survival of cancer cells in a drug tolerant state. To address this point, we compared the transcriptomes of PDX tumors from three CBP-treated and mock-treated CBP-sensitive PDX models (O3312, O1047, O5588) at the end of treatment by clustering and identification/annotation of the differentially expressed genes (Figure S6). Hierarchical clustering showed first a separation of different PDX models and, at a second level, distinguished CBP-treated from mock-treated samples (Figure 3A). Differential gene expression analysis (using Rankproduct algorithms, see Supplementary Information) identified 1333 genes (444 overexpressed and 889 underexpressed) when CBP-treated residual tumors were compared with mock-treated tumors (Figure 3B). Functional annotation was done using with GSEA [15]. Genes underexpressed in residual tumors were involved in cell cycle control, mitosis and proliferation, whereas overexpressed genes were involved in the interferon and inflammation response, as well as epithelial-mesenchymal transition (EMT), *TNF/NFϰB* and fibrosis signatures (Figure 3B, Figure S5A). These changes in gene expression induced by CBP-treatment in our PDX models *in vivo* also overlapped with publicly available gene expression data of platinum-treated HGOC cell lines (Figure S5B) [6],[16]. In addition to activation of EMT pathway genes, cancer stem cell genes (*PROM1*, *ALDH1A3* and *CD44*) and pluripotency transcription factor genes (*SOX2* and *KLF4*) were also overexpressed in residual CBP-sensitive PDX tumors (Figure 3C, D). Consistent with the highly significant overexpression of *SOX2*, 122/444 (27%) of overexpressed genes in residual PDX tumors were known SOX2 transcriptional targets [16] (Figure 3E).

We wondered if an "Embryonic diapause program", a stress-induced stage of dormancy initially identified in development, and recently reported in treatment-persistent colon and breast cancer cells [11],[12], was present in the transcriptomes of our residual PDX tumor. Analyzing residual PDX tumor gene expression data, we found hallmarks of embryonic diapause (Figure 3F, Figure S6A), such as underexpression of cell cycle and metabolism signatures, supporting that the diapause gene expression program was present in post-treatment residual tumor cells in our models.

Acquired-resistance is not associated with major transcriptome changes but shares the overexpression of 3 genes with residual tumors.

In the majority of patients with CBP-sensitive HGOC, the disease recurs within 5 years and recurrences remain sensitive to CBP until they eventually develop resistance. We wondered to what extent the tumors with acquired resistance were related to residual tumors and whether the transcriptional pathways activated in residual tumors were in link with the emergence of resistance. To address this question, we treated recurrent tumors from PDX O8378 and O3312 with repeated cycles of CBP until the tumors finally grew under treatment and generated models with acquired resistance to CBP (Figure 4). Two cycles of treatment were sufficient to obtain resistance in model O8378, whereas three were needed for model O3312. To identify the genes associated with acquired resistance, we compared the transcriptomes of the mock-treated O3312 and O8378 PDXs with those of acquired-resistance models (Figure S6C). Only 16 genes were differentially expressed (9 overexpressed and 7 under-expressed, Figure S6B). Principal Components Analysis showed that the transcriptomes of the residual tumors were strikingly different from those at other stages. In addition, acquired resistant tumors did not present a major transcriptome shift from naïve or mock-treated tumors (Figure 5A). Next, we searched whether transcriptomes of residual and acquired-resistance tumors presented some overlap. We found that, of the 9 genes overexpressed in acquired-resistance tumors, 3 (*CEACAM6*, *CRYAB* and *SOX2*) were also present in the genes overexpressed in post-treatment residual tumors (Figure 5B). These three genes are potentially relevant to the development of resistance to CBP. *CEACAM6* was previously implicated in resistance of ovarian cancer to chemotherapy [17], *CRYAB* was implicated in apoptosis regulation [18] and *SOX2* is well known for its role in stem cell maintenance, as well as the phenotypic identity of drug-resistant cancer cells [9,19,20,21]. To determine whether increased expression of these three genes was associated with poor prognosis, we analyzed publicly available HGOC transcriptomes (Kaplan-Meier plotter, https://kmplot.com, [22]) and searched for the correlation with reported disease outcome. HGOCs expressing all three genes at high levels presented significantly shorter progression-free survival (PFS) when compared with HGOCs expressing low levels (Figure 5C): 80% of the tumors expressing high levels showed clinical progression within 28 months, whereas in tumors expressing low levels this interval was 60 months (HR=1.89, p-value= 4.1 x 10^{-7}). Considered individually, overexpression of *CEACAM6*, *CRYAB* or *SOX2* was also associated with reduced PFS, but the differences between high and low expressors were smaller than when the expression of all 3 genes were combined (Figure S7). Altogether, these data suggest that the joint overexpression of *CEACAM6*, *CRYAB* and *SOX2* may represent a biomarker to predict recurrence and emergence of resistance in CBP-sensitive HGOC.

CEACAM6, CRYAB and SOX2 proteins are markers of residual and CBP-resistant tumors
We investigated the CEACAM6, CRYAB and SOX2 protein expression patterns by IHC in tissue sections of mock-treated, residual, recurrent and acquired resistant tumors from the six CBP-sensitive PDX models with specific antibodies. PAX8 protein expression was also determined to identify areas of HGOC cells. Sections of CBP-treated residual PDXs showed strong cytoplasmic staining for CEACAM6 and CRYAB, and nuclear staining for SOX2 in most tumor cells (Figure 6A and B, Figure S8A, S8B). Nuclear localization of SOX2 was indicative of the transcriptionally active form of the protein (Figure 6B). As in residual tumors, tissue sections of tumors that had acquired CBP resistance stained intensely for CEACAM6, CRYAB and SOX2 in most tumor cells of PDX O3312 (Figure 6A) and PDX O8378 (Figure S9A), even in absence of CBP treatment. Contrastingly, five of the six mock-treated PDX models tested, showed weak CEACAM6 staining, scattered staining in less than 1% of tumor cells for CRYAB and no SOX2 staining (Figure 6A and Figure S9A). However, mock-treated PDX O3312 presented focal clusters of SOX2-positive cells (Figure 6A). Similar staining patterns were found in sections of the primary patient tumor from which O3312 was derived, suggesting pre-existing cell foci expressing SOX2 in this tumor (Figure S10). In confirmation of the transcriptome results, overexpression of these three markers was not maintained upon regrowth in recurrent tumors: in PDX O3312 (Figure 6A) and PDX O8378 (Figure S8) the staining patterns for CEACAM6, CRYAB, SOX2 in recurrent tumors were similar to those in mock-treated PDX tumors.

Together these data indicate that strong CEACAM6, CRYAB and SOX2 staining is a marker of CBP-treated residual HGOC tumor cells and of tumors that acquired resistance.

Discussion

Despite 80% positive initial response to CBP-based therapy, most HGOC patients recur within 6–24 months [1] and a majority of these recurrent tumors remain sensitive to platinum. Patients can go through several cycles of recurrence and chemotherapy, until acquisition of resistance [2]. The biological basis of the CBP-sensitivity of HGOC recurrences remains poorly understood. Very few tumors are biopsied during or immediately after CBP treatment. We used HGOC PDX models [13] to investigate tumor response to CBP and sampled tumors before and after treatment, upon recurrence and after resistance was acquired. We characterized the residual tumors remaining after treatment and compared them with recurrent and resistant tumors.

We and others have shown that PDX reproduced genetic and phenotypic characteristics of the tumor they stem from [13],[23],[24]. Here, we observed that our PDX models also reproduced with remarkable precision the response to CBP, even in absence of a fully competent immune system, which is the principal limitation of PDX models. Moreover, treated residual CBP-sensitive PDXs presented features such as scattered foci of non-proliferating tumor cells embedded in a massive fibrotic mesh, previously observed in biopsies of treatment responsive High Grade Serous Ovarian Carcinoma [25]. In contrast, treated intrinsic CBP-resistant PDXs showed maintained cell proliferation upon CBP treatment. Our findings are, thus, consistent with the observation that increased cell proliferation in neoadjuvant chemotherapy-treated HGOC is associated with reduced progression-free survival and resistance [26].

The build-up of fibrotic tissue observed exclusively in the treated CBP-sensitive PDX models may correspond to an activation of stroma, possibly involving cancer associated fibroblasts (CAF), induced by tumor cells that have undergone EMT [27],[28],[29]. Interestingly, an increase of stromal content, associated to EMT and pro-inflammatory response has been reported in HGSOC that have undergone neo-adjuvant chemotherapy [30],[31]. Furthermore, among the 4 molecular subgroup described in HGOC [32], the mesenchymal subgroup, rich in stroma and showing a high level of desmoplasia is associated with poor survival. Noticeably, a phenotypic shift from non-mesenchymal to the mesenchymal subgroup has been described associated with acquired resistance [5]. It has been proposed that the stromal environment could contribute to the survival of residual tumor cells and partially protect them by limiting the penetration of the chemotherapeutic agent [4,10,33,34]. Therapeutic

approaches minimizing the fibrotic reaction may, thus, improve CBP-response of chemosensitive HGOC [30],[35],[36],[37],[38].

We analyzed the transcriptomes of treated residual, recurrent and acquired resistant PDX models to identify the biological pathways activated or repressed in the response to CBP treatment and gain insight on the mechanisms underlying the acute response to CBP, as well as those contributing to drug tolerance. Illustrating the acute response of tumor cells to CBP, post-treatment residual tumors presented deeply modified transcriptomes characterized by strongly upregulated interferon-response, TNFα and EMT pathways, combined with downregulation of the E2F and mTOR pathways. These changes are consistent with those observed in Drug Tolerant Persister (DTP) cells from various cancer types [11],[12],[39],[40]. Furthermore, residual CBP-sensitive tumor cells were quiescent and viable, another characteristic of DTP [40]. The DTP state is a non-genetic and reversible program that allows cancer cells to cope with chemotherapy-induced stress [40]. Accordingly, we noted that the transcriptomes of CBP-sensitive PDX residual tumors presented a number of hallmarks of the embryonic diapause program which is activated in DTP (Figure S6) [11],[12],[41]. We also noted the up-regulation of the cancer stem cells (CSC) genes *PROM1/CD133* and *ALDH1A3*, and of several EMT-associated genes, previously observed in CBP-treated HGOC cell lines and patient samples [9],[42].

In agreement with previous reports showing that the transcriptomes of recurring HGSOC tumors do not differ substantially from those of their primary counterparts, recurrent CBP-sensitive PDX tumors had very similar transcriptomes to those of mock-treated tumors [5],[43].

Similarly, PDX tumors with acquired CBP-resistance presented little difference with mock-treated controls showing only 16 differentially expressed genes. Of these, 3 genes (*CEACAM6, CRYAB* and *SOX2*) were overexpressed in both residual and acquired-resistance tumors. Each of these three genes has previously been associated with cancer aggressiveness and all are induced under stress condition. *CRYAB* encodes a small heat shock protein that is induced in response to hypoxic and genotoxic stress [44]. Interestingly, its overexpression was associated with inhibition of apoptosis in cisplatin-treated ovarian cancer cell lines and with a poor outcome in HGSOC patients [18,45]. Interestingly, increased CRYAB expression could predict progression free survival in several cancer types [18]. *CEACAM6* (also called *CD66c*) encodes a multi-functional membrane glycoprotein that binds integrin receptors and other members of the CEA (carcinoembryonic antigen) family and can induce reorganization

of the extracellular matrix [46]. It is also a marker of carcinogen-induced genotoxic stress [46]. Attenuation of *CEACAM6* expression in a cisplatin-treated lung cancer cell line was associated with reduced expression of the mesenchymal marker *VIM* and of *SOX2*, which encodes a transcription factor that, together with *OCT4* and *NANOG,* is crucial for pluripotent stem cells induction [17]. The increased *SOX2* expression that we observed in residual and acquired-resistance tumors is consistent with its reported up-regulation in platinum treated ovarian cancer cell lines, which may be related to the proposed role of *SOX2* in CSC maintenance and reduced apoptotic response of HGOC cells exposed to platinum salts [9], [19],[42],[20]. Importantly, we noted that 122 of the 444 genes overexpressed in residuals HGOC PDX were identified SOX2 transcriptional targets, hence, reinforcing the idea that overexpression of *SOX2* could play a prominent role in HGOC response to CBP.

Altogether, these data strongly suggest that *CEACAM6, CRYAB* and *SOX2* participate in the response of tumor cells to platinum by attenuating the apoptotic response, reorganizing the extracellular matrix and favoring the EMT, as well as promoting the acquisition of stem cell features. We propose that CEACAM6, CRYAB and SOX2 may participate in the emergence of acquired CBP-resistance in HGOC. This is in line with the strong association of *CEACAM6, CRYAB* and *SOX2* overexpression with adverse HGOC patient outcome. These three gene were overexpressed in tumors that had acquired resistance. None of the four untreated intrinsically CBP-resistant PDX (O3053, O2815, O3111 and 03264) showed strong simultaneous CEACAM6, CRYAB or SOX2 staining (Figure S9), suggesting that the overexpression of these genes does not account for intrinsic CBP resistance in HGOC

Our findings indicate that the recurrence of CBP-sensitive HGOC results from the survival of a small population of transiently quiescent cancer cells. Similar observations were made by Pajic and coworkers [47] who, using a Brca1-/-;p53-/- mouse mammary tumor model, showed that cisplatin treatment failed to eliminate some slow cycling cells leaving behind non cycling drug-tolerant remnants that ultimately favored tumor recurrence. These residual cells may develop complex interactions with their stroma to induce a strong fibrotic reaction and adopt a drug-tolerant persister-like gene expression program, including the overexpression of *CEACAM6, CRYAB* and *SOX2*. The mechanisms governing the overexpression of these genes in residual tumors and their re-induction during acquisition of CBP resistance are unclear at present. Whether it is caused by adaptative stress signaling [40,48] or results from the selection of rare cells that express these genes at basal levels in non-treated tumors remains to be determined. Our data suggest that both mechanisms may co-exist in CBP-sensitive HGOC:

we observed isolated SOX2- and/or CRYAB-positive tumor cells before treatment in one PDX model (O3312) and its corresponding patient tumor. Emergence of CBP resistance in this particular model may, thus, result from the gradual selection of a subset of SOX2-positive cells. Conversely, SOX2- or CRYAB-positive cells were absent in the remaining five CBP-sensitive, non-treated PDXs, suggesting a progressive transcriptional switch leading to sustained levels of *CEACAM6, CRYAB* and *SOX2* expression possibly as an adaptative stress signaling. It will, thus, be interesting to determine whether *CRYAB*, *CEACAM6* and *SOX2* are co-regulated or regulate each other, as suggested by reports indicating that attenuation of *CEACAM6* expression resulted in the down-regulation of *SOX2* [21] and beyond to identify a master switch governing their re-expression in CBP-treated HGOC.

In conclusion, our findings indicate that the recurrence of CBP-sensitive HGOC is due to the survival of a small population of transiently quiescent cancer cells embedded in a fibrotic mesh in residual tumors and expressing *CEACAM6, CRYAB* and *SOX2*.

Data availability statement

All expression profiling data are publicly available under GSE198701

References

1.   Bowtell DDL. The genesis and evolution of high-grade serous ovarian cancer. *Nat Rev Cancer*. 2010, 10:803–8.

2.   Colombo P-E, Fabbro M, Theillet C, Bibeau F, Rouanet P, Ray-Coquard I. *Crit Rev Oncol Hematol*. 2013, 22:1–10.

3.   Heitz F, Harter P, Åvall-Lundqvist E, Reuss A, Pautier P, Cormio G, et al. Early tumor regrowth is a contributor to impaired survival in patients with completely resected advanced ovarian cancer. An exploratory analysis of the Intergroup trial AGO-OVAR 12. *Gynecologic Oncology*. 2019, 152:235–42.

4.   Chien J, Kuang R, Landen C, Shridhar V. Platinum-sensitive recurrence in ovarian cancer: the role of tumor microenvironment. *Front Oncol*. 2013, 3:251.

5.   Patch A-M, Christie EL, Etemadmoghadam D, Garsed DW, George J, Fereday S, et al. Whole–genome characterization of chemoresistant ovarian cancer. *Nature*. 2015, 52:1489–94.

6.   Miow QH, Tan TZ, Ye J, Lau JA, Yokomizo T, Thiery JP, et al. Epithelial-mesenchymal status renders differential responses to cisplatin in ovarian cancer. *Oncogene*. 2015, 34:1899–907.

7.   Galluzzi L, Senovilla L, Vitale I, Michels J, Martins I, Kepp O, et al. Molecular mechanisms of cisplatin resistance. *Oncogene*. 2012, 31:1869–83.

8.   Dai Y, Jin S, Li X, Wang D. The involvement of Bcl-2 family proteins in AKT-regulated cell survival in cisplatin resistant epithelial ovarian cancer. *Oncotarget*. 2017, 8:1354–68.

9.   Robinson M, Gilbert SF, Waters JA, Lujano-Olazaba O, Lara J, Alexander LJ, et al. Characterization of SOX2, OCT4 and NANOG in Ovarian Cancer Tumor-Initiating Cells. *Cancers (Basel)*. 2021, 13:262.

10. Rottenberg S, Disler C, Perego P. The rediscovery of platinum-based cancer therapy. *Nat Rev Cancer*. 2021, 21:37–50.

11. Dhimolea E, de Matos Simoes R, Kansara D, Al'Khafaji A, Bouyssou J, Weng X, et al. An Embryonic Diapause-like Adaptation with Suppressed Myc Activity Enables Tumor Treatment Persistence. *Cancer Cell*. 2021,39:240–256.e11.

12. Rehman SK, Haynes J, Collignon E, Brown KR, Wang Y, Nixon AML, et al. Colorectal Cancer Cells Enter a Diapause-like DTP State to Survive Chemotherapy. *Cell*. 2021, 184:226–242.e21.

13.   Colombo P-E, Manoir du S, Orsett B, Bras-Gonçalves R, Lambros MB, Mackay A, et al. Ovarian carcinoma patient derived xenografts reproduce their tumor of origin and preserve an oligoclonal structure. *Oncotarget*. 2015, 6:28327–40.

14.   Chaves-Moreira D, Morin PJ, Drapkin R. Unraveling the Mysteries of PAX8 in Reproductive Tract Cancers. *Cancer Res*. 2021, 81:806–10.

15.   Subramanian A, Tamayo P, Mootha VK, Mukherjee S, Ebert BL, Gillette MA, et al. Gene set enrichment analysis: a knowledge-based approach for interpreting genome-wide expression profiles. *Proc Natl Acad Sci USA*. 2005, 102:15545–50.

16.   Kuleshov MV, Jones MR, Rouillard AD, Fernandez NF, Duan Q, Wang Z, et al. Enrichr: a comprehensive gene set enrichment analysis web server 2016 update. *Nucleic Acids Res*. 2016, 44: 90–7.

17.   Du H, Li Y, Sun R, Yuan Y, Sun S, Zhang Y. CEACAM6 promotes cisplatin resistance in lung adenocarcinoma and is regulated by microRNA-146a and microRNA-26a. *Thorac Cancer*. 2020, 11:2473–82.

18.   Volkmann J, Reuning U, Rudelius M, Häfner N, Schuster T, Becker V Ros A, et al. High expression of crystallin αB represents an independent molecular marker for unfavourable ovarian cancer patient outcome and impairs TRAIL- and cisplatin-induced apoptosis in human ovarian cancer cells. *Int J Cancer*. 2013, 132:2820–32.

19.   Wen Y, Hou Y, Huang Z, Cai J, Wang Z. SOX2 is required to maintain cancer stem cells in ovarian cancer. *Cancer Sc*i. 2017, 108:719–31.

20.   Bareiss PM, Paczulla A, Wang H, Schairer R, Wiehr S, Kohlhofer U, et al. SOX2 expression associates with stem cell state in human ovarian carcinoma. *Cancer Res*. 2013, 73:5544–55.

21.   Sharma A, Cao EY, Kumar V, Zhang X, Leong HS, Wong AML, et al. Longitudinal single-cell RNA sequencing of patient-derived primary cells reveals drug-induced infidelity in stem cell hierarchy. *Nat Commun*. 2018, 9:4931.

22.   Györffy B, Lanczky A, Eklund AC, Denkert C, Budczies J, Li Q, et al. An online survival analysis tool to rapidly assess the effect of 22,277 genes on breast cancer prognosis using microarray data of 1,809 patients. *Breast Cancer Res Treat*. 2010, 123:725–31.

23.   Tudrej P, Kujawa KA, Cortez AJ, Lisowska KM. Characteristics of in Vivo Model Systems for Ovarian Cancer Studies. *Diagnostics*. 2019, 9:120.

24.   Alkema NG, Wisman GBA, van der Zee AGJ, van Vugt MATM, de Jong S. Studying platinum sensitivity and resistance in high-grade serous ovarian cancer: Different models for different questions. *Drug Resist Updat*. 2016, 24:55–69.

25.   Böhm S, Faruqi A, Said I, Lockley M, Brockbank E, Jeyarajah A, et al. Chemotherapy Response Score: Development and Validation of a System to Quantify Histopathologic Response to Neoadjuvant Chemotherapy in Tubo-Ovarian High-Grade Serous Carcinoma. *J Clin Oncol*. 2015, 33:2457–63.

26. Pölcher M, Friedrichs N, Rudlowski C, Fimmers R, Keyver-Paik M-D, Kübler K, et al. Changes in Ki-67 labeling indices during neoadjuvant chemotherapy for advanced ovarian cancer are associated with survival. *Int J Gynecol Cancer*. 2010, 20:555–60.

27. Dongre A, Weinberg RA. New insights into the mechanisms of epithelial-mesenchymal transition and implications for cancer. *Nat Rev Mol Cell Biol*. 2019, 20:69–84.

28. Loret N, Denys H, Tummers P, Berx G. The Role of Epithelial-to-Mesenchymal Plasticity in Ovarian Cancer Progression and Therapy Resistance. *Cancers (Basel)*. 2019 11:838.

29. Mieulet V, Garnier C, Kieffer Y, Guilbert T, Nemati F, Marangoni E, et al. Stiffness increases with myofibroblast content and collagen density in mesenchymal high grade serous ovarian cancer. *Sci Rep*. 2021, 11:4219.

30. Leary A, Genestie C, Blanc-Durand F, Gouy S, Dunant A, Maulard A, et al. Neoadjuvant chemotherapy alters the balance of effector to suppressor immune cells in advanced ovarian cancer. *Cancer Immunol Immunother*. 2021, 70:519–31.

31. Westergaard MCW, Milne K, Pedersen M, Hasselager T, Olsen LR, Anglesio MS, et al. Changes in the Tumor Immune Microenvironment during Disease Progression in Patients with Ovarian Cancer. *Cancers (Basel)*. 2020, 12:3828.

32. Tothill RW, Tinker AV, George J, Brown R, Fox SB, Lade S, et al. Novel molecular subtypes of serous and endometrioid ovarian cancer linked to clinical outcome. *Clin Cancer Res*. 2008, 14:5198–208.

33. Trédan O, Galmarini CM, Patel K, Tannock IF. Drug resistance and the solid tumor microenvironment. *J Natl Cancer Inst.*. 2007, 99:1441–54.

34. Provenzano PP, Cuevas C, Chang AE, Goel VK, Hoff Von DD, Hingorani SR. Enzymatic targeting of the stroma ablates physical barriers to treatment of pancreatic ductal adenocarcinoma. *Cancer Cell*. 2012, 21:418–29.

35. Yeung T-L, Leung CS, Li F, Wong SST, Mok SC. Targeting Stromal-Cancer Cell Crosstalk Networks in Ovarian Cancer Treatment. *Biomolecules*. 2016, 6:3.

36. Givel A-M, Kieffer Y, Scholer-Dahirel A, Sirven P, Cardon M, Pelon F, et al. miR200-regulated CXCL12β promotes fibroblast heterogeneity and immunosuppression in ovarian cancers. *Nat Commun.* 2018, 9:1056.

37. Zhao Y, Cao J, Melamed A, Worley M, Gockley A, Jones D, et al. Losartan treatment enhances chemotherapy efficacy and reduces ascites in ovarian cancer models by normalizing the tumor stroma. *Proc. Nat. Acad. Sci. USA*. 2019, 116:2210–9.

38. Huang J, Zhang L, Wan D, Zhou L, Zheng S, Lin S, et al. Extracellular matrix and its therapeutic potential for cancer treatment. *Signal Transduct Target Ther*. 2021, 6:153.

39. Thakur B, Ray P. Cisplatin triggers cancer stem cell enrichment in platinum-resistant cells through NF-κB-TNFα-PIK3CA loop. *J Exp Clin Cancer Res*. 2017, 22:1–14.

40. De Conti G, Dias MH, Bernards R. Fighting Drug Resistance through the Targeting of Drug-Tolerant Persister Cells. *Cancers (Basel)*. 2021, 13:1118.

41. Bulut-Karslioglu A, Biechele S, Jin H, Macrae TA, Hejna M, Gertsenstein M, et al. Inhibition of mTOR induces a paused pluripotent state. *Nature*. 2016, 540:119–23.

42. Wang Y, Zhao G, Condello S, Huang H, Cardenas H, Tanner EJ, et al. Frizzled-7 Identifies Platinum-Tolerant Ovarian Cancer Cells Susceptible to Ferroptosis. *Cancer Res*. 2021, 81:384–99.

43. Kreuzinger C, Geroldinger A, Smeets D, Braicu EI, Sehouli J, Koller J, et al. A Complex Network of Tumor Microenvironment in Human High-Grade Serous Ovarian Cancer. *Clin Cancer Res*. 2017, 23:7621–32.

44. Zhang J, Liu J, Wu J, Li W, Chen Z, Yang L. Progression of the role of CRYAB in signaling pathways and cancers. *Onco Targets Ther*. 2019,12:4129–39.

45. Yang M, Li Y, Tian F. Association between Alpha B-crystallin expression and prognosis in patients with solid tumors: A protocol for systematic review and meta-analysis. *Medicine*. 2021, 100:e24831.

46. Johnson B, Mahadevan D. Emerging Role and Targeting of Carcinoembryonic Antigen-related Cell Adhesion Molecule 6 (CEACAM6) in Human Malignancies. *Clin Cancer Drugs*. 2015, 2:100–11.

47. Pajic M, Blatter S, Guyader C, Gonggrijp M, Kersbergen A, Küçükosmanoğlu A, et al. Selected Alkylating Agents Can Overcome Drug Tolerance of G0-like Tumor Cells and Eradicate BRCA1-Deficient Mammary Tumors in Mice. *Clin Cancer Res*. 2017, 23:7020–33.

48. Pazarentzos E, Bivona TG. Adaptive stress signaling in targeted cancer therapy resistance. *Oncogene*. 2015, 34:5599–606.

49. Boroviak, T., Loos, R., Lombard, P., Okahara, J., Behr, R., Sasaki, E., Nichols, J., Smith, A., and Bertone, P. Lineage-specific profiling delineates the emergence and progression of naive pluripotency in mammalian embryogenesis. *Dev. Cell*. 2015, 35, 366–382.

50. Jacot W, Lopez-Crapez E, Mollevi C, Boissière-Michot F, Simony-Lafontaine J, Ho-Pun-Cheung A, et al. BRCA1 Promoter Hypermethylation is Associated with Good Prognosis and Chemosensitivity in Triple-Negative Breast Cancer. *Cancers (Basel)*. 2020, 12: 828.

51. Junqueira LC, Bignolas G, Brentani RR. Picrosirius staining plus polarization microscopy, a specific method for collagen detection in tissue sections. *Histochem J*. 1979, 11:447–55.

52. Bankhead P, Loughrey MB, Fernandez JA, Dombrowski Y, McArt DG, Dunne PD, et al. QuPath: Open source software for digital pathology image analysis. *Sci Rep*. 2017, 7:16878.

References cited in the supplementary information [49], [50], [51], [52]

PDX data					Patient data			
PDX-ID	PDX treatment	Response	time to recurrence in mice (days)	PDX *BRCA1* status	histo-type	Figo Stage	RFS in patient (days)	Clinical Response
O3053	CBP	Progression	NA	WT	High grade serous	IIIC	230	Resistant
O2815	CBP	Progression	NA	WT	Carcinosarcoma	IIIC	119	Resistant
O3111	CBP	Stable	NA	WT	High grade serous	IIIC	138	Resistant
O3264	CBP	Stable	NA	WT	Carcinosarcoma	IIIC	PUT*	Resistant
O3312	CBP	Regression	70	Meth	High grade serous	IIIC	412	Sensitive
O8378	CBP	Regression	50	WT	High grade serous	IIIC	353	Sensitive
O7876	CBP	Regression	40	WT	High grade serous	IIIC	901	Sensitive
O5588	CBP	Regression	30	Mut	High grade serous	IIIC	669	Sensitive
O1047	CBP	Regression	100	Mut	High grade serous	IV	4365	Sensitive
O4571	CBP	Regression	150	Meth	High grade serous	IIIC	2998	Sensitive

Table 1: Principal characteristics of the 10 HGOC PDX models tested. PDX treated with CBP were coded regression in case of tumor volume reduction, progression when tumor volumes increased or stable if tumor did not change. Time to recurrence in the animal corresponds to the mean time in several animals monitored in parallel. *BRCA1* status is indicated as wild type (WT), coding mutation (Mut), promoter hypermethylation (Me). PDX were all from High Grade carcinomas and at minimum Figo Stage IIIC. Patients recurrence free survival (RFS) is expressed in days starting after end of chemo. * Patient O3264 progressed under treatment (PUT).

Figure Legends

Figure 1: High Grade Ovarian Carcinoma PDX treated with carboplatin (CBP) recapitulate the clinical response observed in patients. A- Growth curves of the 10 PDX models (4 corresponding to clinically resistant noted CBP-resistant, 6 from clinically responsive noted CBP-sensitive) over the 4 weeks of treatment. Each curve corresponds to the average tumor volume of at least 8 treated animals. Tumor volumes were normalized on tumor volume at treatment start. Curves from the 4 CBP-resistant PDXs are indicated in orange, red, beige and brown, those of the 6 CBP-sensitive models in green and blue. **B-** Growth curves of CBP-sensitive PDX models after end of treatment. Models showed complete regression and were monitored for up to 270 days to determine tumor recurrence. Color code of the curves is same as in panel A **C-** Non-responsive and sensitive models show distinctly different proliferation rates under treatment. Tissue section from 4week mock and CBP-treated PDXs were stained for the cell proliferation marker Ki-67 and the rate of Ki-67-positive cells scored in each model before and after 4 weeks of treatment.

Figure 2: Residual tumor cells in treated CBP-sensitive tumors are embedded in a fibrotic mesh. A: PAX8 staining of two CBP-sensitive PDX before (left panel) and after treatment (right panel). Cells showing strong nuclear PAX8 staining correspond to human ovarian carcinoma cells. Before treatment PDXs show large areas of tumor cells with embedded islets of mouse stroma (fibroblasts). After CBP treatment, cancer cells showing aberrant and sometimes multinucleated nuclei form small clusters embedded in the stroma. Magnification refers to the microscope lens used. **B:** Picro-Sirius Red staining reveals massive fibrosis after CBP treatment in sensitive PDXs. Whole tumor mount of CBP-res PDX O3053 and 4 CBP-sensitive PDXs O8378, O7876, O1047, O4571 are presented. Red stained areas correspond to collagen dense (fibrosis) formations. In untreated PDX, Sirius Red staining is mostly restricted to the periphery of the tumor or small islands. After treatment, fibrosis occupies a large fraction of the tumor in CBP-sensitive models, whereas no major change in localization or extension of the fibrosis was observed in CBP-res models. **C:** High magnification of two CBP-sensitive PDXs. Serial sections stained with Sirius Red (left) and PAX8 antibody (red), note that after treatment residual cancer cells are included in a dense fibrosis network.

Figure 3: Residual CBP-sensitive tumors have gene expression profiles indicative of proliferation downregulation and of inflammation and Epithelial-Mesenchymal Transition upregulation. A- Clustering (Ward) of the 3 CBP-Sensitive PDXs, individual PDX models cluster together and treated and untreated samples are separated. **B-** Annotation of differentially expressed genes in residual tumors *versus* untreated PDX. A combined analysis using a percentage of false positive < 0.05 as a threshold and rank product method (R Package RankProd) uncovered 889 overexpressed and 444 underexpressed genes. Differentially expressed genes were annotated with GSEA, Hallmark and GO gene sets and revealed a global repression of proliferation associated genes in residual cells and the activation of genes involved in interferon signaling, epithelial-to-mesenchymal transition (EMT) and fibrosis, inflammation and apoptosis. All p values $< 10^{-10}$ (details can be seen in Figure S5). **C-** Cancer Stem Cell and pluripotency transcription factors overexpressed in residual PDX. **D-** *SOX2* mRNA levels are increased in residual compared with mock-treated PDX. **E-** Transcriptional targets of SOX2, RELA, SMAD2 were scored among the 444 overexpressed genes in residual PDX and indicate that 27.4% correspond to SOX 2 targets. Indicated pvalue corresponds to an adjusted pvalue **F-** Gene set enrichment analysis (GSEA) depicting transcriptional changes in CBP-treated residual PDXs versus mock-treated PDXs

(O3312, O1047, O5588). A Diapause signature is clearly present (NES =-2.11, FDR <0.001). Enrichment for other genesets which are hallmarks of the Diapause program are presented in Figure S6.

Figure 4: *In vivo* **selection of HGOC PDX with acquired CBP resistance from two models. A**: Treatment scheme, mice received 2 intra-peritoneal injection of 50mg/kg CBP per week for 4 weeks. The same scheme was applied at each cycle of treatment. **B**: Growth curves of PDX O8378 during the first (left) and second (right) cycle of treatment (each line indicates 3 different tumors growing on different mice). **C**: For O3312, 3 cycles of treatment were necessary to reach resistance.

Figure 5: Acquired-resistance is not associated with major transcriptome changes but shares the overexpression of 3 genes with residual tumors. A: Principal Component Analysis of treatment naive, residual, recurrence and resistant tumors. **B:** Overlap between overexpressed genes in residual and acquired-resistant PDX tumors (using untreated PDX as a reference) identified 3 genes in common. **C:** Kaplan-Meier progression free survival curves of primary HGOC stratified according to joint expression levels of *CRYAB, CEACAM6* and *SOX2*. Tumors with high expression of the three genes recur earlier.

Figure 6: CEACAM6, CRYAB and SOX2 proteins are markers of residual and CBP-resistant tumors. Immunostained proteins are indicated on top. **A:** Sections of O3312 PDX model and its original patient tumor (Primary T.). Exposure to CBP and experimental conditions are indicated on the left. PDX Ctrl correspond to mock-treated tumors. PDX CBP goes for sections of CBP-treated residual PDX sampled after 4 weeks of treatment. PDX Recur correspond to PDX that have regrown after treatment end. PDX Resis correspond to O3312 PDX with acquired-resistance. **B:** Serial sections of the same residual tumor from PDX O1047. Pictures were taken at different magnifications indicated on the left. Square 1 is the location of X20 magnification, Square 2 that of X63 magnification.
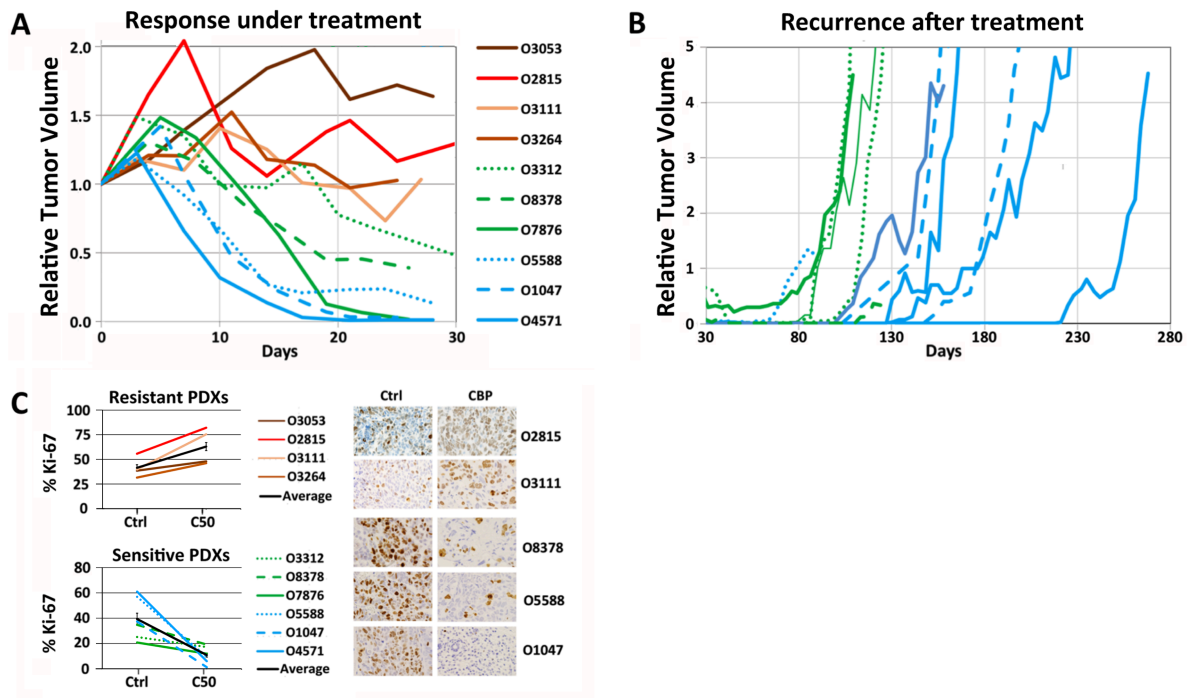
Figure 1: High Grade Ovarian Carcinoma PDX treated with carboplatin (CBP) recapitulate the clinical response observed in patients. A- Growth curves of the 10 PDX models (4 corresponding to clinically resistant noted CBP-resistant, 6 from clinically responsive noted CBP-sensitive) over the 4 weeks of treatment. Each curve corresponds to the average tumor volume of at least 8 treated animals. Tumor volumes were normalized on tumor volume at treatment start. Curves from the 4 CBP-resistant PDXs are indicated in orange, red, beige and brown, those of the 6 CBP-sensitive models in green and blue. **B-** Growth curves of CBP-sensitive PDX models after end of treatment. Models showed complete regression and were monitored for up to 270 days to determine tumor recurrence. Color code of the curves is same as in panel A **C-** Non-responsive and sensitive models show distinctly different proliferation rates under treatment. Tissue section from 4week mock and CBP-treated PDXs were stained for the cell proliferation marker Ki-67 and the rate of Ki-67-positive cells scored in each model before and after 4 weeks of treatment.
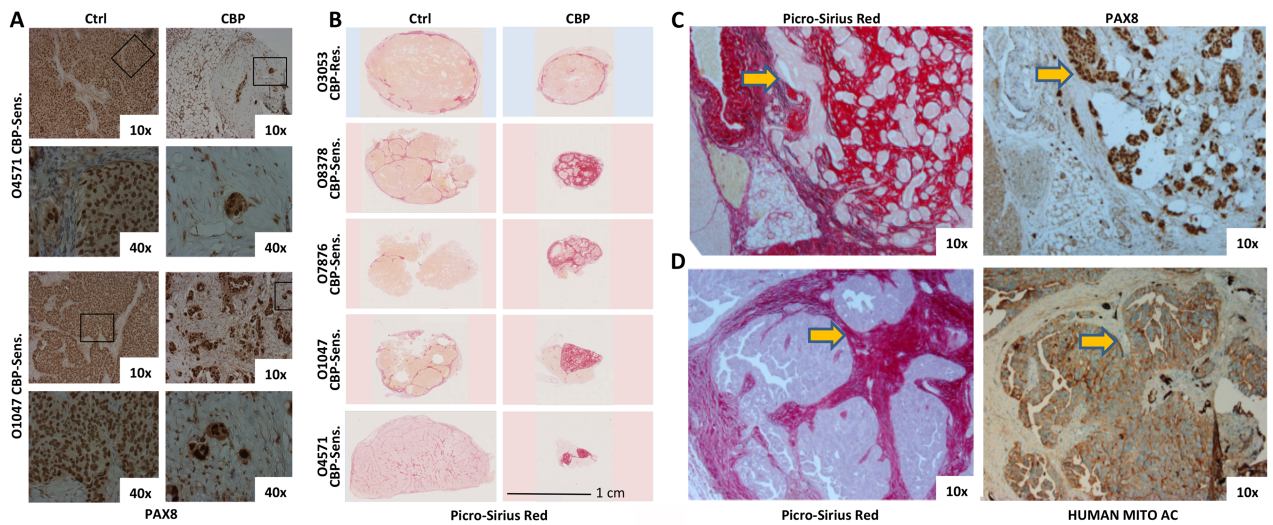
Figure 2: Residual tumor cells in treated CBP-sensitive tumors are embedded in a fibrotic mesh. A: PAX8 staining of two CBP-sensitive PDX before (left panel) and after treatment (right panel). Cells showing strong nuclear PAX8 staining correspond to human ovarian carcinoma cells. Before treatment PDXs show large areas of tumor cells with embedded islets of mouse stroma (fibroblasts). After CBP treatment, cancer cells showing aberrant and sometimes multinucleated nuclei form small clusters embedded in the stroma. Magnification refers to the microscope lens used. **B:** Picro-Sirius Red staining reveals massive fibrosis after CBP treatment in sensitive PDXs. Whole tumor mount of CBP-res PDX O3053 and 4 CBP-sensitive PDXs O8378, O7876, O1047, O4571 are presented. Red stained areas correspond to collagen dense (fibrosis) formations. In untreated PDX, Sirius Red staining is mostly restricted to the periphery of the tumor or small islands. After treatment, fibrosis occupies a large fraction of the tumor in CBP-sensitive models, whereas no major change in localization or extension of the fibrosis was observed in CBP-res models. **C**: High magnification of two CBP-sensitive PDXs. Serial sections stained with Sirius Red (left) and PAX8 antibody (red), note that after treatment residual cancer cells are included in a dense fibrosis network.

A

B Genes differentially expressed in treated CBP-sens PDXs

444 overexpressed
1- IFNg response
2- IFNa response
3- EMT/fibrosis
4- TNFa
5- Inflammation
6- KRAS pathway

889 underexpressed
1- Cell cycle
2- E2F targets
3- Mitosis
4- MYC targets
5- mTORC1 signaling

C

CSC and Pluripotency TF in the 444 overexpressed genes			
CSC	Rank	Fold Change	p value
PROM1	24	2.46	0
ALDH1A3	48	2.63	0
CD44	176	2.07	0.0001
Pluripotency TF			
KLF4	242	1.77	0.0002
SOX2	354	1.54	0.0006

D SOX2

E

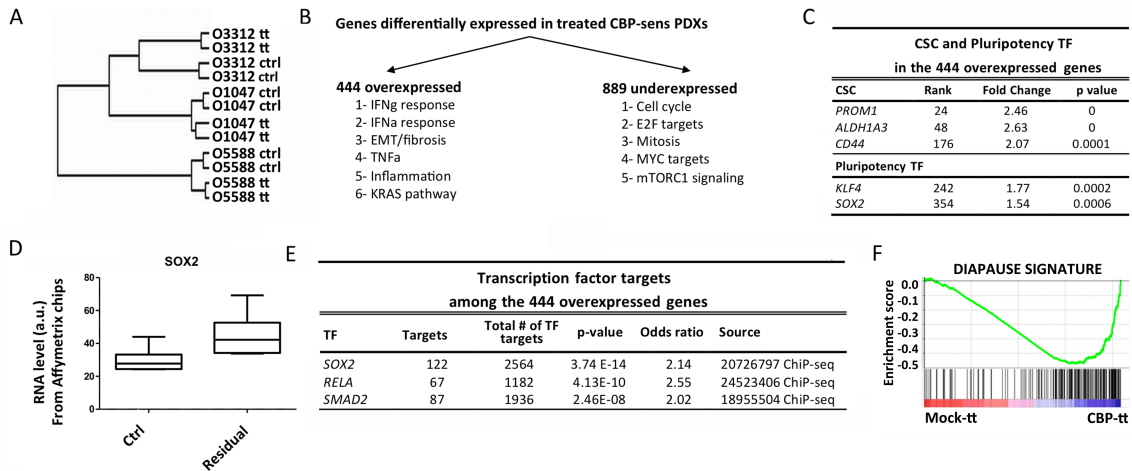| Transcription factor targets among the 444 overexpressed genes					
TF	Targets	Total # of TF targets	p-value	Odds ratio	Source
SOX2	122	2564	3.74 E-14	2.14	20726797 ChiP-seq
RELA	67	1182	4.13E-10	2.55	24523406 ChiP-seq
SMAD2	87	1936	2.46E-08	2.02	18955504 ChiP-seq

F DIAPAUSE SIGNATURE

Figure 3: Residual CBP-sensitive tumors have gene expression profiles indicative of proliferation downregulation and of inflammation and Epithelial-Mesenchymal Transition upregulation. A- Clustering (Ward) of the 3 CBP-Sensitive PDXs, individual PDX models cluster together and treated and untreated samples are separated. **B-** Annotation of differentially expressed genes in residual tumors *versus* untreated PDX. A combined analysis using a percentage of false positive < 0.05 as a threshold and rank product method (R Package RankProd) uncovered 889 overexpressed and 444 underexpressed genes. Differentially expressed genes were annotated with GSEA, Hallmark and GO gene sets and revealed a global repression of proliferation associated genes in residual cells and the activation of genes involved in interferon signaling, epithelial-to-mesenchymal transition (EMT) and fibrosis, inflammation and apoptosis. All p values $< 10^{-10}$ (details can be seen in Figure S5). **C-** Cancer Stem Cell and pluripotency transcription factors overexpressed in residual PDX. **D-** *SOX2* mRNA levels are increased in residual compared with mock-treated PDX. **E-** Transcriptional targets of SOX2, RELA, SMAD2 were scored among the 444 overexpressed genes in residual PDX and indicate that 27.4% correspond to SOX 2 targets. Indicated pvalue corresponds to an adjusted pvalue **F-** Gene set enrichment analysis (GSEA) depicting transcriptional changes in CBP-treated residual PDXs versus mock-treated PDXs
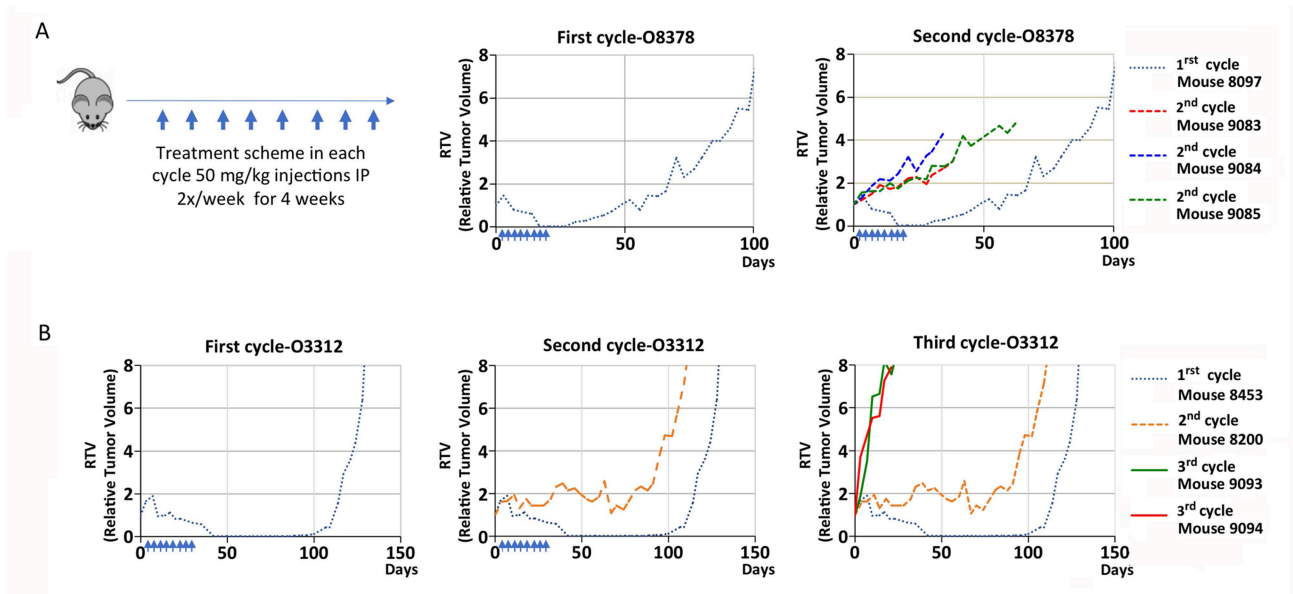
Figure 4: *In vivo* selection of HGOC PDX with acquired CBP resistance from two models. A: Treatment scheme, mice received 2 intra-peritoneal injection of 50mg/kg CBP per week for 4 weeks. The same scheme was applied at each cycle of treatment. **B**: Growth curves of PDX O8378 during the first (left) and second cycle (right) of treatment (each line indicates 3 different tumors growing on different mice). **C**: For O3312, 3 cycles of treatment were necessary to reach resistance.
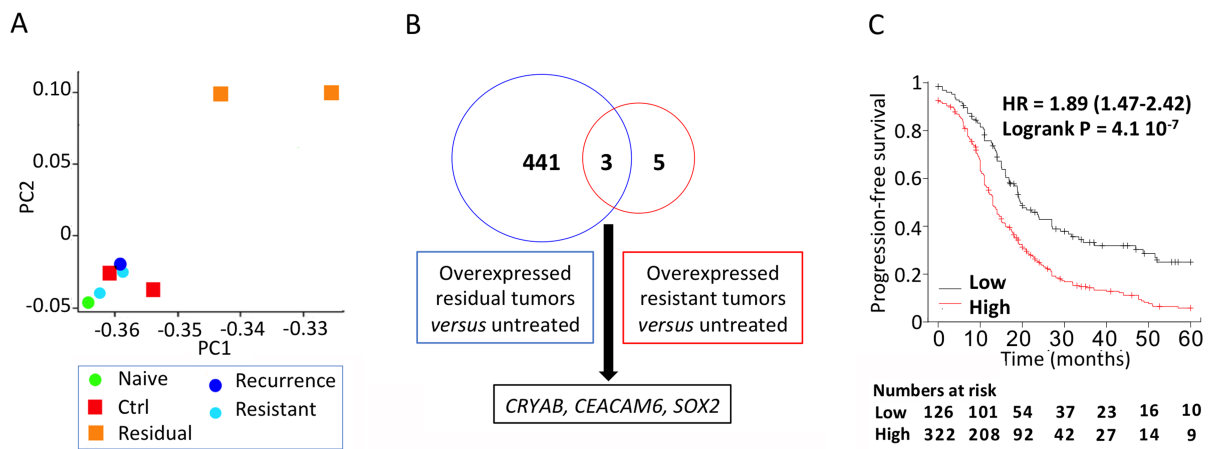
Figure 5: Acquired-resistance is not associated with major transcriptome changes but shares the overexpression of 3 genes with residual tumors. A: Principal Component Analysis of treatment naive, residual, recurrence and resistant tumors. **B:** Overlap between overexpressed genes in residual and acquired-resistant PDX tumors (using untreated PDX as a reference) identified 3 genes in common. **C:** Kaplan-Meier progression free survival curves of primary HGOC stratified according to joint expression levels of *CRYAB, CEACAM6* and *SOX2*. Tumors with high expression of the three genes recur earlier.
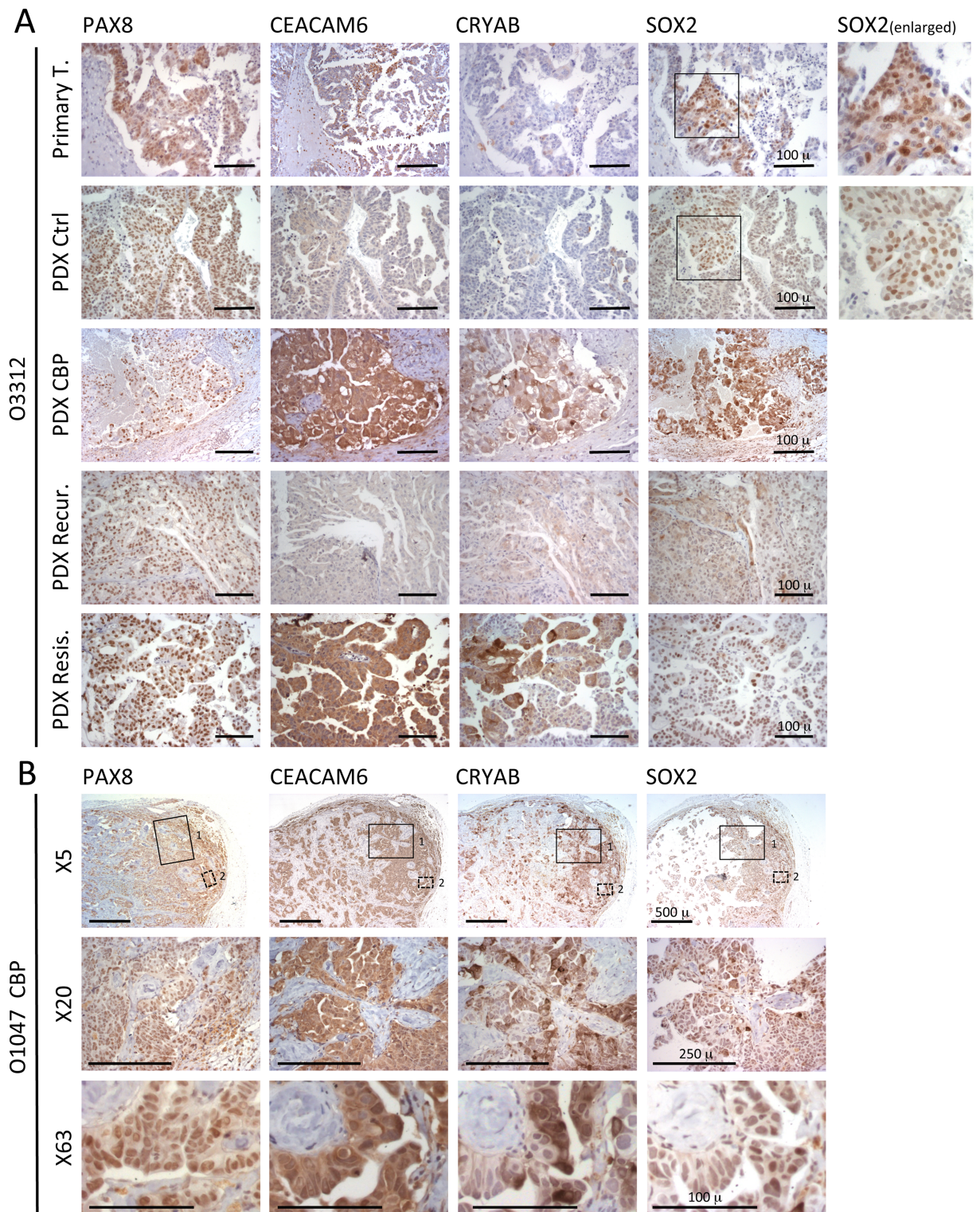
Figure 6: CEACAM6, CRYAB and SOX2 proteins are markers of residual and CBP-resistant tumors. Immunostained proteins are indicated on top. **A:** Sections of O3312 PDX model and its original patient tumor (Primary T.). Exposure to CBP and experimental conditions are indicated on the left. PDX Ctrl correspond to mock-treated tumors. PDX CBP goes for sections of CBP-treated residual PDX sampled after 4 weeks of treatment. PDX Recur correspond to PDX that have regrown after treatment end. PDX Resis correspond to O3312 PDX with acquired-resistance. **B:** Serial sections of the same residual tumor from PDX O1047. Pictures were taken at different magnifications indicated on the left. Square 1 is the location of X20 magnification, Square 2 that of X63 magnification.

Supplementary information :

Materials and Methods

HGOC PDX models and in vivo treatment

Establishment of PDX collection : The 10 PDX models used were previously established (Colombo et al, 2015) and are described in Supplementary Table 1. The study was reviewed and approved by the ethics committees for animal experimentations of the University of Montpellier (CEEA-LR-12028). Briefly, fresh ovarian cancer samples were collected from the pathology department and macro-dissected by the pathologist. Samples were transferred to the animal facility and implanted within a maximum of 60 min after surgical removal. A fragment of tumor (~8 mm3) was implanted into the inter-scapular fat pad of 3-4-week-old female Swiss-nude mice. Tumors were passaged onto a further cohort of mice before graft volume reached 1600 mm^3. After four passages PDX models were frozen in 10 DMSO for long term storage. At this stage, human stroma was replaced by mouse stroma, but overall PDXs showed excellent conservation of the gross histological features observed in the human tumor of origin. In addition we demonstrated that PDXs showed a good conservation of transcriptomic and subclonal composition of the tumors they stemmed from. All HGOC PDXs used in this study were PAX8 positive. Routine histological analysis was done by the Pathology Department of ICM.

PDX Amplification step : For the current experiments, frozen PDXs fragments 50 mm^3 were thawed and grafted into the inter-scapular fat pad of 3 to 6 3-4 week old Swiss-nude female mice (Charles Rivers, Larbresle, France). Tumor volume was monitored by caliper measurements. After tumor growth, fragments were grafted on about 30 mice.

Initial CBP treatment : when tumor reached 100-150mm^3 mice were selected and randomly distributed in the different experimental arms. The present study comprised two experimental arms; Carboplatin-treated (CBP-) and mock-treated comprising 7 to 10 mice in each arm. Treatment consisted of 2 intra-peritoneal (IP) injections per week for 4 weeks with either saline solution (mock) or with 50 mg/kg CBP (Fresenius Kabi, Sèvres, France). At the end of treatment, some mice were either euthanized to collect tumor samples for further histological and transcriptome analyses or kept to monitor relapse. Effect of this initial treatment is shown in Fig. 1A. For transcriptome analyses of residual tumors, samples were snap-frozen in liquid nitrogen. For histological analyses, samples were fixed in buffered 10 % paraformaldehyde for 48 hours and embedded in paraffin according to standard procedures.

<u>Follow-up of relapses :</u> at the end of initial treatment, some mice showing complete macroscopic regression were monitored for tumor relapse. Relapse always occurred at the same anatomical location in the inter-scapular fat pads. Tumor volume was measured by caliper once a week for up to 9 months.

In vivo <u>generation resistant tumors</u> : recurring tumors from sensitive PDXS, after initial complete macroscopic regression upon initial treatment, were passaged to further mice. They were subjected to variable number of cycles of CBP 50mg/kg (2 intra-peritoneal (IP) injections per week for 4 weeks with either saline solution (mock) or with 50 mg/kg CBP) upon absence of response to treatment. Examples are presented in Fig. 4 in which resistance occurred after one cycle (O8378) or two cycles (O3312).

Transcriptome analysis

<u>RNA extraction and raw data generation:</u> RNAs were extracted from frozen tumor fragments collected after one month (one cycle of CBP or mock-treated) at the end of the initial treatment (residual tumors), after first regrowth (recurrence) and after acquisition of resistance (acquired-resistant tumors) using RNeasy Mini Kit (Qiagen, Les Ulis, France). The latter were not under treatment. Expression profiling was performed on Affymetrix Human Genome GeneChip U133Plus2 at the MGX-transcriptome platform (BioCampus-IRMB) according to the manufacturer's recommendation. Raw feature data were normalized using Robust Multi-array Average (RMA) method (R package Affy).

<u>Clustering :</u> Non-supervised hierarchical clustering was done using Pearson metric and Pairwise Average-Linkage (HierarchicalClustering command, Genepattern software; https://cloud.genepattern.org). Consensus clustering gave similar results aggregating first PDX models and then CBP-treated/Mock-treated PDXs (ConsensusClustering command).

<u>Differentially expressed genes (DEG) and annotation:</u> DEG between residual tumors paired with mock-treated tumors were identified using the rank product methods (R Package"RankProd") with threshold percentage of false positive < 0.05 in combined comparison of mock/CBP-treated for O3312, O1047 and O5588 specifying PDXs of origin (See Figure S6C). To do so, we defined the origin parameter (argument of RPadvance instruction) in three classes corresponding to the three PDXs and the cl argument as treated or untreated in the RPadvance instruction. Thus, RP can perform an overall analysis combining three PDXs datasets together (See RankProd tutorial, R Package"RankProd").

This analysis identified 444 overexpressed genes and 889 underexpressed genes in CBP-treated vs. residual tumors (percentage of false positive < 0.05) with p-value < 0.002 and p-value < 0.003

respectively for each group differentially expressed genes. DEG were annotated with GSEA using two gene sets : Hallmark and GO gene sets (www.gsea-msigdb.org/gsea/index.jsp) as seen in Figure 4B. Over-expressed genes (444 genes in residual tumor) were further annotated with Enrich tools (https://amp.pharm.mssm.edu/Enrichr/; (Kuleshov et al. 2016), as seen in Figure 3E.

To analyze if signatures associated with DIAPAUSE were present in residual tumors, we used GSEA analyses after retrieving datasets (from www.gsea-msigdb.org/gsea/index.jsp) found to be underexpressed in Diapause tumors by Dhimolea E. et al. (2021) namely Hallmark_MYC_TARGET_V1, REACTOME_TRANSLATION, MTORC1-SIGNALING, GOBP_OXYDATIVE_PHOSPHORYLATION. We also retrieved a mouse embryonic diapause dataset (Boroviak et al. 2015). The GSEA analyses were performed using the GSEA software (Subramanian et al., 2005) version version 4.1.0.3 based on the pre-ranked option (Subramanian et al. 2005). To generate the ranklist, we use gene fold-change calculated between the average of the residual tumors and the average of the mock-treated tumors. For the visualizations we use the GSEA enrichment scores (ES) and the gene set size normalized enrichment scores (NES) Figure 3E and Figure S6).

Differentially expressed genes between resistant and mock-treated tumors were identified using the rank product methods (R Package"RankProd") with threshold percentage of false positive < 0.05 and in combined comparison of mock treated/acquired-resistant tumors for O3312 and O8378 specifying PDXs of origin. To do so, we defined the origin parameter (argument) in two classes corresponding to the three PDXs and the cl argument as treated or untreated in the RPadvance instruction. Thus, RP can perform an overall analysis combining three PDXs datasets together (See RankProd tutorial).
 Nine (9) genes were found to be overexpressed in resistant tumor versus mocked-treated tumors with a pfp < 0.05. This threshold (percentage of false positive < 0.05) corresponds for the 9 overexpressed genes pvalue < 0.00003).

<u>Survival analysis :</u> We used the kmplot tools on line to evaluate if expression of individual genes or the mean of three genes (*CEACAM6, CRYAB* and *SOX2*) and selected Serous Ovarian Cancer (Kaplan-Meier plotter, [https://kmplot.com,](https://kmplot.com)) with the option Auto select best cutoff. This tool allows the exploration of a compendium of datasets namely GSE14764 (n=80), GSE15622 (n=35), GSE18520 (n=63), GSE19829 (n=28), GSE23554 (n=28), GSE26193 (n=107), GSE26712 (n=195), GSE27651(n=49), GSE30161(n=58), GSE3149 (n =116), GSE51373 (n=28), GSE63885 (n= 101), GSE65986 (n=55), GSE9891(n = 285), TCGA (n=565). This analysis was done with all datasets available at the date of consultation of the web site (mars 2021).

Exome sequencing analysis

Tumor DNA from sensitive PDXs were sequenced on the HiSeq using the Illumina standard exomic sequencing protocol based upon the Agilent SureSelect 50Mb V4 probe capture set and passed through CASAVA QC. Paired end reads were aligned to the human genome (hg19) with BWA using largely default parameters - Illumina PHRED scores and allowing single gaps and small Indels. BAM files from BWA were then run through the GATK Best Practice Variant Calling pipeline (v2), recalibrating and realigning around SNPs and Indels using dbSNP130. Variants tumor genomes were recorded in variant Call Format (VCF) and annotated with the Variant Effect Predictor script (ensembl). Meaningful results are presented in Table S1.

BRCA1 promoter methylation status : DNA methylation patterns at the CpG islands of the _BRCA1_ promoter were assessed, using the MS-PCR assay as previously described (Jacot et al. 2020). This method distinguishes between unmethylated and hypermethylated alleles on the basis of sequence changes following bisulfite treatment of DNA, that converts unmethylated cytosines to uracil. Bisulfite treatment was performed using the EpiTect Bisulfite Kit (Qiagen GmbH, Hilden, Germany). PCRs were performed on an Eppendorf Mastercycler (Eppendorf, Hamburg, Germany), with the EpiTect MSP-PCR Kit (QIAGEN GmbH, Hilden, Germany), 6-FAM™-labeled or HEX™-labeled forward primers, amplifying specifically hypermethylated or unmethylated _BRCA1_ DNA sequences, respectively. This MS-PCR analyzed a total of seven CpG sites, located at −37, −29, −21, −19, +16, +19, and +27, relative to the _BRCA1_ exon 1A transcription start site. The primers for the methylated reaction generated a 75-bp-long amplicon and the primers for the unmethylated amplified an 86-bp-long product. The EpiTect PCR Control DNA Set (Qiagen Hindel, Germany), containing both bisulfite-converted methylated and unmethylated DNA and unconverted unmethylated DNA, were also added as MS-PCR controls. DNA fragment analysis was performed by capillary electrophoresis on an Applied Biosystems 3130 Genetic Analyzer. Analyses were conducted with the GeneMapper Software v3.7 (Apllied Biosystems, Foster City, CA, USA).

Histology and Immunohistochemical procedures

Fibrosis was detected using PicroSirius Red staining of Collagen fibers (Junqueira et al. 1979). Immunochemistry was performed on 3μm formaldehyde fixed deparaffinized tissue-sections, rehydrated and treated for 30 min in boiling EDTA (pH 9) or Citrate buffer (pH 6) for antigen retrieval. The following primary antibodies were used to detect PAX8 (10336-1-AP, Proteintech, Manchester, UK; dilution: 1/200); CRYAB (HPA057100-100ul, Sigma-Aldrich, Saint-Quentin-Fallavier, France); dilution 1/50, SOX2 (AB5603, Sigma-Aldrich, dilution : 1/500), CEACAM6 (ab134074, Sigma-Aldrich, dilution 1/200). Neutralization of endogenous peroxidase was done with H_2O_2 0.3% for 20 min, followed by saturation of unspecific sites with 20% horse serum. Sections were then incubated with primary antibodies or mouse isotype control (Mouse IgG1κ, Sigma–Aldrich) overnight at 4 °C. Sections were washed 3X in 0.1% Tween20-PBS solution at 25 °C for 15min and

incubated 30min with secondary antibodies (Biotinylated Goat anti-Rabbit IgG, BA-1000, Vector Laboratories-Cliniscience, Nanterre, dilution 1/500), washed 3X in 0.1% Tween20-PBS solution at 25 °C and signal amplification using the VECTASTAIN Elite ABC System ABC kit (PK-6100, Vector Laboratories-CliniSciences, Nanterre, France Vector) and 3,3-diaminobenzidine substrate (PK-4100, Vector Laboratories-CliniSciences). Slides were counterstained with hematoxylin, dehydrated and mounted.

IHC for KI67, human mitochondria and cleaved caspase were performed on a VENTANA Discovery Ultra automated staining instrument (Ventana Medical-Systems, Narcastet, France). The following primary antibodies were used to detect KI67 (SP6, #M3064, Spring Bioscience, Ventana Narcastet, France; dilution: 1/250,), human mitochondria, (MAB1273, #113-1, Merck Millipore, Saint-Quentin-Fallavier, France; dilution: 1/200); Cleaved caspase (ASP176, #9661S, Cell Signaling, Ozyme, St Cyr l'Ecole; dilution 1/400). Slides were developed using the DISCOVERY OmniMap anti-rabbit HRP detection Kit (cat# 05269679001, Ventana) or the HQ conjugated antibody anti-rabbit IgG (cat# 07017812001, Ventana) followed by an HRP conjugated anti-HQ antibody (cat# 07017936001, Ventana) according to the manufacturer's instructions. Stained slides were digitalized using a NanoZoomer scanner (Hamamatsu, Massy, France).

Ki-67 scoring : IHC signals were quantified using the QuPath v0.2.3-software (Bankhead et al. 2017). Two or three tumors when available were analyzed for each condition and three independent fields by tumors. In average, the number of evaluated nuclei was 75300 by PDX condition (The minimal number of nuclei was 771 for the smallest residual tumor). We used the positive cell detection instruction with the optical sum density and a minimum size of 200 and others parameters as defaults.

CEACAM6, CRYAB, SOX2 scoring : IHC signals were quantified using the QuPath v0.2.3-software. Three independent fields by tumors were used for evaluation. We used the positive cell detection instruction with the optical sum density and a minimum size of 200 and Nucleus or cytoplasm DAB OD for SOX2 nuclear, CRYAB cytoplasmic and CEACAM6 membrane staining. H-score calculated (H score formula: 3 x percentage of strongly stained cells + 2 x percentage of moderately stained cells + percentage of weakly staining cells, giving a range of 0 to 300), was determined within QuPath v0.2.3-software (Figure S9 and S10).

Reference to Supplementary Figures:

1. Kuleshov MV, Jones MR, Rouillard AD, Fernandez NF, Duan Q, Wang Z, et al. Enrichr:

a comprehensive gene set enrichment analysis web server 2016 update. Nucleic Acids Res. 2016 Jul 8;44(W1):W90–7.

2. Boroviak, T., Loos, R., Lombard, P., Okahara, J., Behr, R., Sasaki, E., Nichols, J., Smith, A., and Bertone, P. (2015). Lineage-specific profiling delineates the emergence and progression of naive pluripotency in mammalian embryogenesis. Dev. Cell 35, 366–382.

3. Subramanian A, Tamayo P, Mootha VK, Mukherjee S, Ebert BL, Gillette MA, et al. Gene set enrichment analysis: a knowledge-based approach for interpreting genome-wide expression profiles. Proc Natl Acad Sci USA [Internet]. 2005 Oct 25;102(43):15545–50. Available from: https://www.pnas.org/content/102/43/15545.long

4. Jacot W, Lopez-Crapez E, Mollevi C, Boissière-Michot F, Simony-Lafontaine J,Ho-Pun-Cheung A, Chartron E, Theillet C, Lemoine A, Saffroy R, Lamy PJ, Guiu S. BRCA1 Promoter Hypermethylation is Associated with Good Prognosis and Chemosensitivity in Triple-Negative Breast Cancer. Cancers. 2020 Mar 30;12(4):828.

5. Junqueira LC, Bignolas G, Brentani RR. Picrosirius staining plus polarization microscopy, a specific method for collagen detection in tissue sections. Histochem J. 1979 Jul;11(4):447–55.

6. Bankhead P, Loughrey MB, Fernandez JA, Dombrowski Y, McArt DG, Dunne PD, et al. QuPath: Open source software for digital pathology image analysis. Scientific Reports [Internet]. 2017 Dec 4;7(1):16878. Available from: https://www.nature.com/articles/s41598-017-17204-5.

PDX data						Patient data								
PDX-ID	Response to CBP	time to recurrence in mice (days)	PDX *BRCA1* status	PDX TP53 mutation	PDX HR gene status	histo-type	Year Surgery	Figo Stage	Nodal involvt	RFS in patient (days)	Clinical Response	NAC at the time of graft	patient status	OVS (days)
O3053	Progression	NA	WT	p.Tyr220Cys		High grade serous	2012	IIIC	N+	230	Resistant	yes	DCD	596
O2815	Progression	NA	WT	ms codon 234		High Grade Carcinosarcoma	2008	IIIC		119	Resistant	no	DCD	211
O3111	Stable	NA	WT	NA		High grade serous	2010	IIIC	N-	138	Resistant	no	DCD	1246
O3264	Stable	NA	WT	ms codon 179		High Grade Carcinosarcoma	2009	IIIC		PUT*	Resistant	yes	DCD	127
O3312	Regression	70	Meth	p.Gly245Ser		High grade serous	2008	IIIC	N+	412	Sensitive	no	DCD	903
O8378	Regression	50	WT	p.Gln192*		High grade serous	2008	IIIC	N+	353	Sensitive	no	DCD	1559
O7876	Regression	40	WT	p.Gln192*		High grade serous	2012	IIIC	N-	901	Sensitive	no	Alive	
O5588	Regression	30	Mut:p.Ser1634 Cys missense	p.Glu339*	BRIP1:p.Thr 630fs	High grade serous	2008	IIIC	N+	669	Sensitive	no	DCD	3198
O1047	Regression	100	Germline deletion exon 8-13	p.Leu679fs		High grade serous	2008	IV	N+	4365	Sensitive	no	Alive	
O4571	Regression	150	Meth	p.Tyr220Cys		High grade serous	2012	IIIC	N+	2998	Sensitive	no	Alive	

Supplementary Table 1: essential clinical information on the primary High Grade Ovarian Carcinomas from which the PDX models used in this study have been derived.

NA= not applicable; Meth= hypermethylation of the *BRCA1* promoter; N+ = nodal invasion; PUT = progression under treatment; DCD = patient deceased.

Legend to Supplementary Figures

Figure S1. Evolution of tumor volumes in the 10 PDX models during treatment (50 mg/Kg, twice per week, 4 weeks)

Figure S2. Percentage of Ki-67 positive nuclei in the tested PDXs

Figure S3. Representative cleaved caspase-3 immunostaining in two PDX models

Figure S4. CBP-sens PDX regress under treatment with a massive fibrosis build up

Figure S5. Modified pathways and annotation of the genes overexpressed in residual PDX

Figure S6. principal pathways modified in post-treatment residual HGPC PDX.

Figure S7. HGOC expressing high levels of CEACAM6 or CRYAB or SOX2 recur earlier than those with low levels

Figure S8. Representative immunostaining for PAX8, CEACAM6, CRYAB and SOX2

Figure S9. CEACAM6, CRYAB and SOX2 immunostaining in non-treated PDX models used in this study

Figure S10. CEACAM6, CRYAB, SOX2 immunostaining patterns in patient tumor O3312

Table S1. Essential clinical information of the primary High Grade Ovarian Carcinomas from which the PDX models used in this study were derived

Stanislas du Manoir et al.

Supplementary Figures
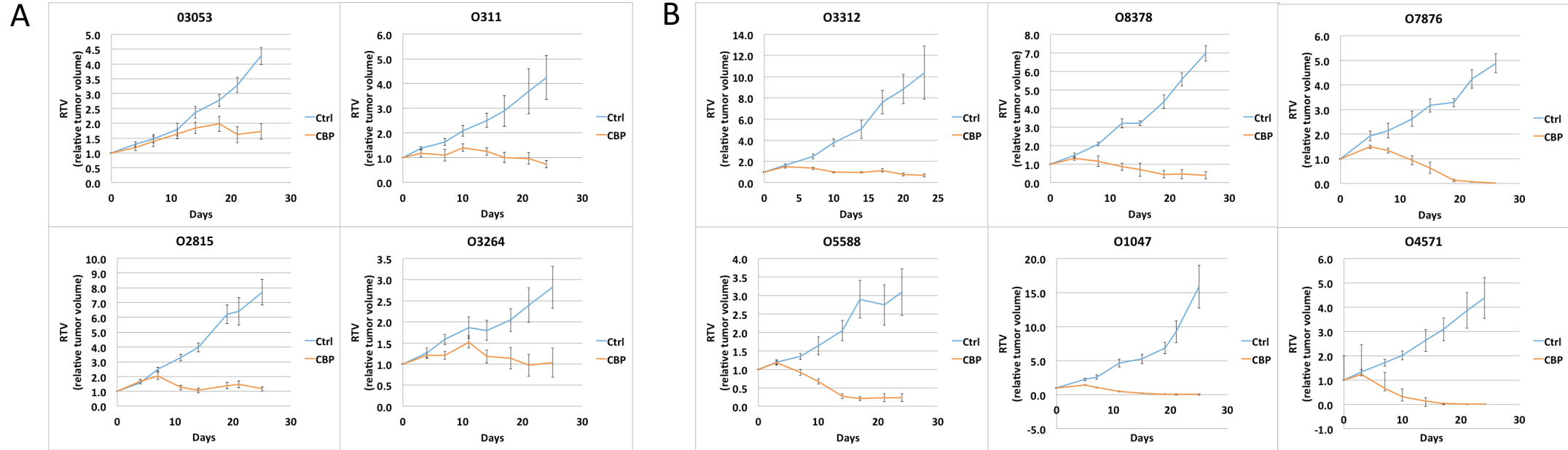
Supplementary Fig. S1 : Evolution of tumor volumes in the 10 PDX models during treatment (50 mg/Kg, twice a week, 4 weeks). A: CBP-Resistant PDXs. **B**: CBP-Sensitive PDXs. In CBP-treated resistant tumors, inflexion points of the RTV curve are between 7-18 days and in CBP-treated sensitive tumors , inflexion points are between 3-5 days.
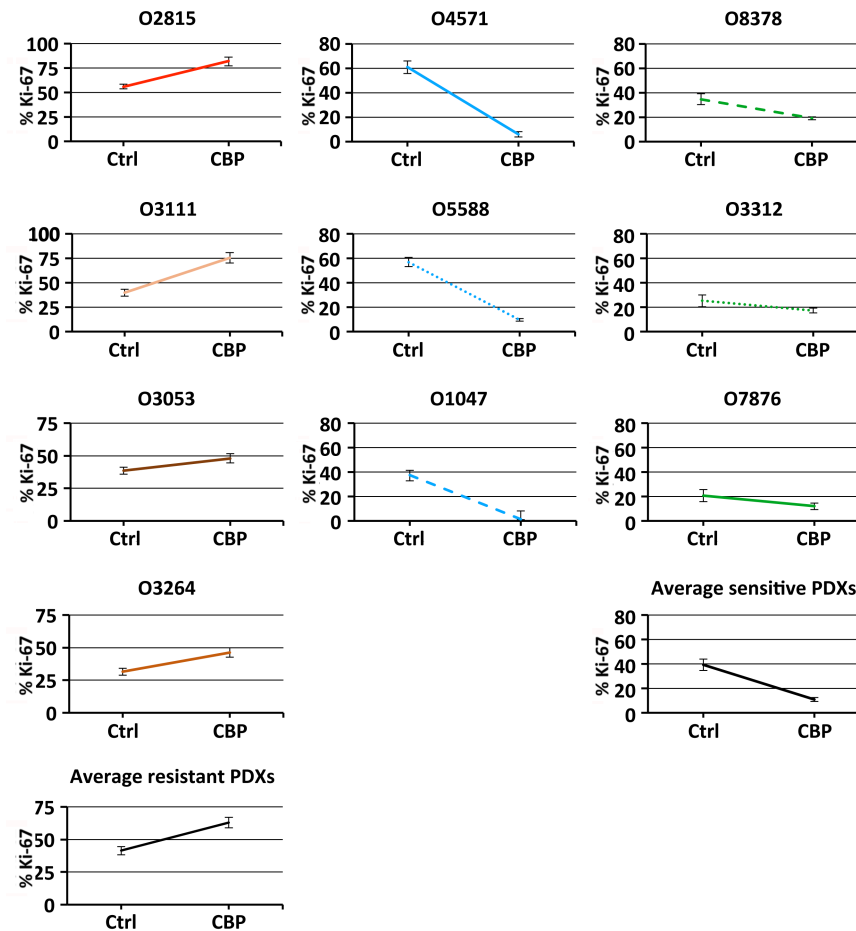
Supplementary Fig. S2: Percentage of Ki-67 positive nuclei in the tested PDXs; mock-treated were compared with CBP-treated. CBP-resistant PDXs showed increased Ki-67 positive nuclei in CBP-treated compared with mock-treated (t-test, Each individual comparison $p < 0.05$, paired t- test of average of resistant models= 0.009).

CBP-sensitive showed reduced Ki-67 positive nuclei in CBP-treated compared with mock-treated PDXs (t-test : individual comparison $p < 0.05$ except for O3312: $p = 0.069$ and O7876: $p = 0.064$, average sensitive PDXs: paired t- test of Average of sensitive PDXs $p=0.0095$)

Quantification was done using the QuPath software (See Materials and Methods for details)

Mock-treated **CBP-treated**

CBP-resistant model O3053

CBP-sensitive model O1047
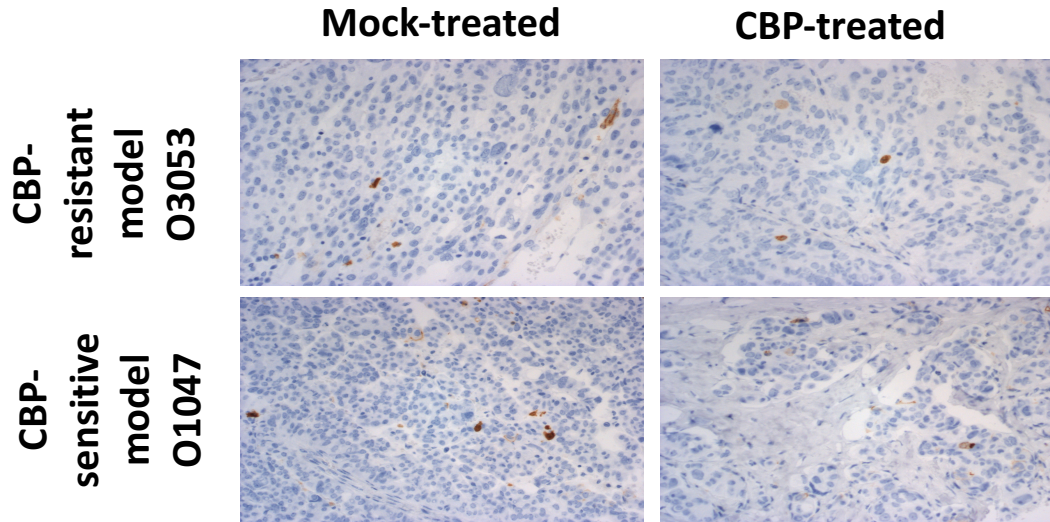
Supplementary Fig. S3: Representative caspase3 immunostaining in two PDX models. PDX O3053 (CBP-resistant model) and PDX 1047 (CBP-sensitive model) were immunostained for caspase 3 expression in mock-treated (left) and CBP treated samples. Caspase3 staining was found in less than 1% in mock-treated and CBP-treated PDXs. Magnification was X20.
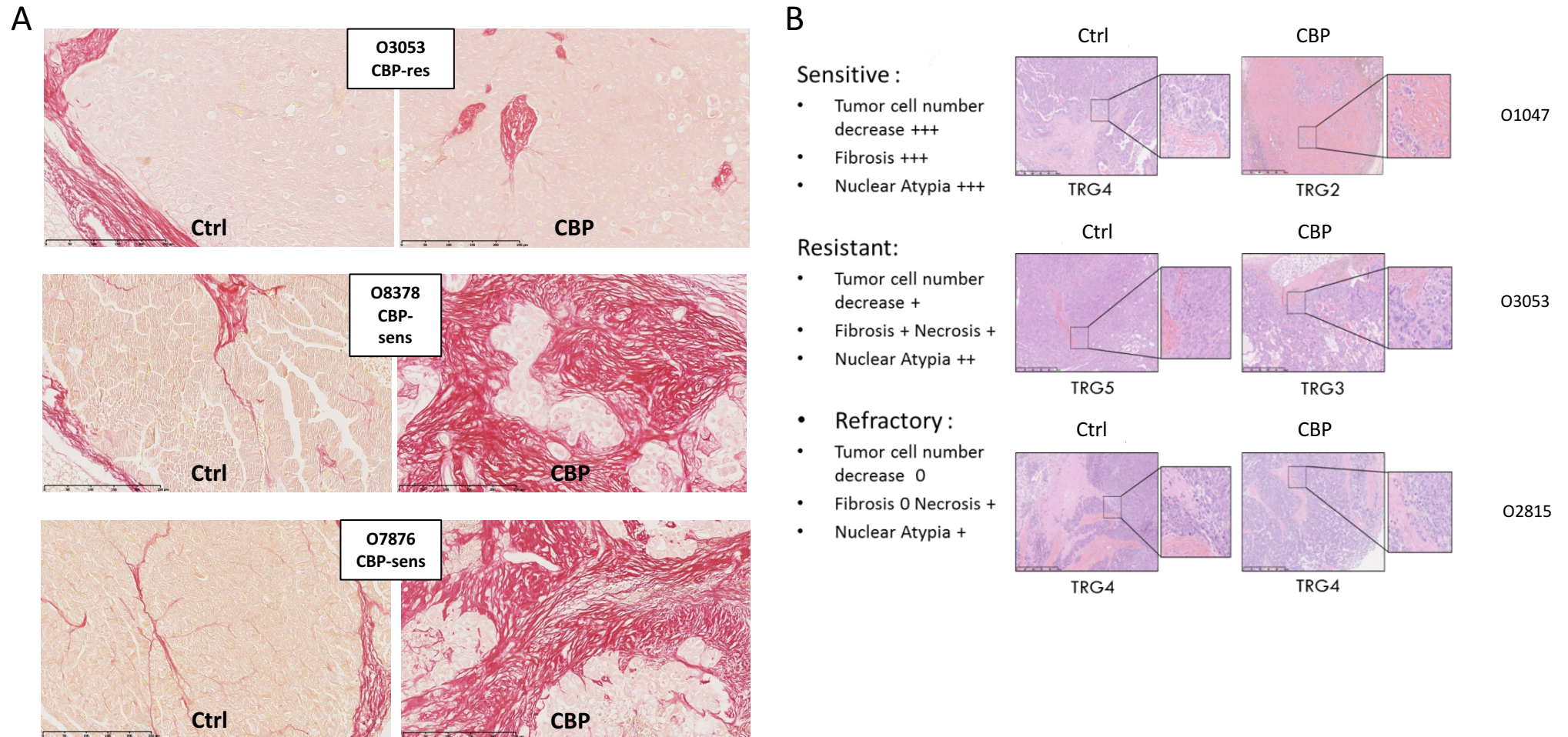
Supplementary Fig. S4: CBP-sens PDX regress under treatment with a massive fibrosis build up. A- Three representative section of one CBP-resistant model (PDX O3053) and two CBP-sensitive (O8378 and O7876). Fibrosis was revealed by Picro-Sirius Red staining in Ctrl and CBP-treated PDXs. **B-** Tumor response was evaluated in three PDX models: (i) CBP-Sensitive (PDX O1047) showed an important decrease in tumor cell number accompanied by extensive fibrosis (ii) CBP-Resistant (PDX O3058) no obvious variation of number of cells and no increase in fibrosis (iii) Refractory (PDX O2815) no obvious variation of number of cells. Note that O2815 is a carcinosarcoma, which showed limited fibrosis prior to treatment and no fibrosis increase after treatment.

A

Annotation of the 444 overexpressed genes in Residual tumors

Gene Set Name	Description	p-value	FDR q-value
HALLMARK INTERFERON GAMMA RESPONSE	Genes up-regulated in response to IFNG [GeneiD-3458].	3.53E-32	1.76E-30
HALLMARK INTERFERON ALPHA RESPONSE	Genes up-regulated in response to alpha interferon proteins.	8.7E-25	2.17E-23
HALLMARK EPITHELIAL MESENCHYMAL TRANSITION	Genes defining epithelial-mesenchymal transition,as in wound healing, fibrosis and	3.97E-15	4.96E-14
HALLMARK TNFA SIGNALING VIA NFKB	Genes regulated by NF-kB in response to TNF [GeneiD=7124].	3.97E-15	4.96E-14
HALLMARK INFLAMMATORY RESPONSE	Genes defining inflammatory response.	4.6E-14	4.6E-13
HALLMARK KRAS SIGNALING UP	Genes up-regulated by KRAS activation.	5.03E-13	4.19E-12
HALLMARK APOPTOSIS	Genes mediating programmed celi death (apoptosis) by activation of caspases.	1.77E-11	1.27E-10
HALLMARK PS3 PATHWAY	Genes involved in p53 pathways and networks.	5.04E-11	3.15E-10

Annotation of the 889 underexpressed gene in Residual tumors with GOBP collection

Gene Set Name	Description	p-value	FDR q-value
GOBP CELL CYCLE	Phases and events that occur in a cell during successive cell replication or nuclear	6.75E-128	5.05E-124
GOBP MITOTIC CELL CYCLE	Progression through the phases of the mitotic cell cycle.	4.92E-115	1.84E-111
GOBP CELL CYCLE PROCESS	The cellular process that ensures successive accurate and complete genome	8.40E-115	2.09E-111
GOBP CHROMOSOME ORGANIZATION	Assembly,arrangement of constituent parts, or disassembly of chromosomes.	1.51E-90	2.83E-87
GOBP CELL DIVISION	The process resulting in division of a cell to form more cells.	2.57E-83	3.84E-80
GOBP CHROMOSOME SEGREGATION	The process in which chromosomes,is organized into specifis structures and then	3.04E-74	3.79E-71
GOBP DNA METABOLIC PROCESS	Any cellular metabolic process involving deoxyribonucleic acid.	2.05E-71	2.19E-68

Annotation of the 889 underexpressed gene in Residual tumors with Hallmark collection

| Gene Set Name	Description	p-value	FDR q-value
HALLMARK E2F TARGETS	Genes encoding cell cycle related targets of E2F transcription factors.	1.59E-117	7.94E-116
HALLMARK G2M CHECKPOINT	Genes involved in the G2/M checkpoint, as in progression through the cell division	1.20E-95	3.00E-94
HALLMARK MYC TARGETS VI	A subgroup of genes regulated by MYC - version 1	1.59E-31	2.66E-30
HALLMARK MITOTIC SPINDLE	Genes important for mitotic spindle assembly.	5.74E-24	6.90E-23
HALLMARK MTORC1 SIGNALING	Genes up-regulated through activation of mTORCcomplex.	6.90E-24	6.90E-23

B

Annotation of 444 overexpressed gene with Drug Perturbations from GEO up with Enrich tool

Term	Overlap	Adj. P-value	Odds Ratio	Combined Score
cisplatin human GSE47856 sample 3153	50/289	4.18E-27	7.8	526
cisplatin human GSE47856 sample 3146	55/392	1.48E-25	6.3	400
cisplatin human GSE47856 sample 3158	59/471	4.54E-25	5.6	349
Interferon beta-1a human GSE26104 sample 3186	55/419	2.22E-24	5.9	354
cetuximab human GSE61495 sample 3133	48/321	1.08E-23	6.7	391
cisplatin human GSE47856 sample 3155	47/312	2.16E-23	6.8	388

Supplementary Fig. S5: Modified pathways and annotation of the genes overexpressed in residual PDX. A: principal pathways (first lines)**. B:** annotation of the 444 overexpressed genes and overlap with existing datasets of genes modified by chemotherapy treatment in Ovarian Cancer cell line dataset, in particular cisplatin. The first six overlapping datasets are presented.
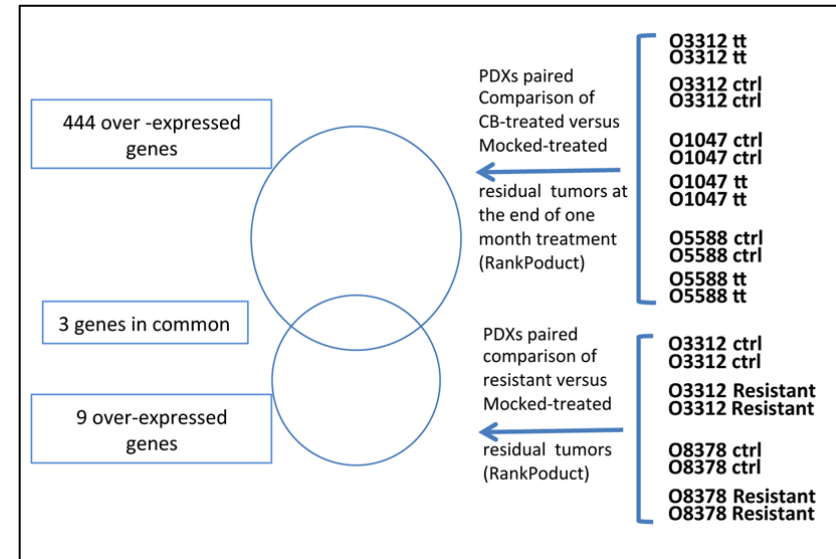
A
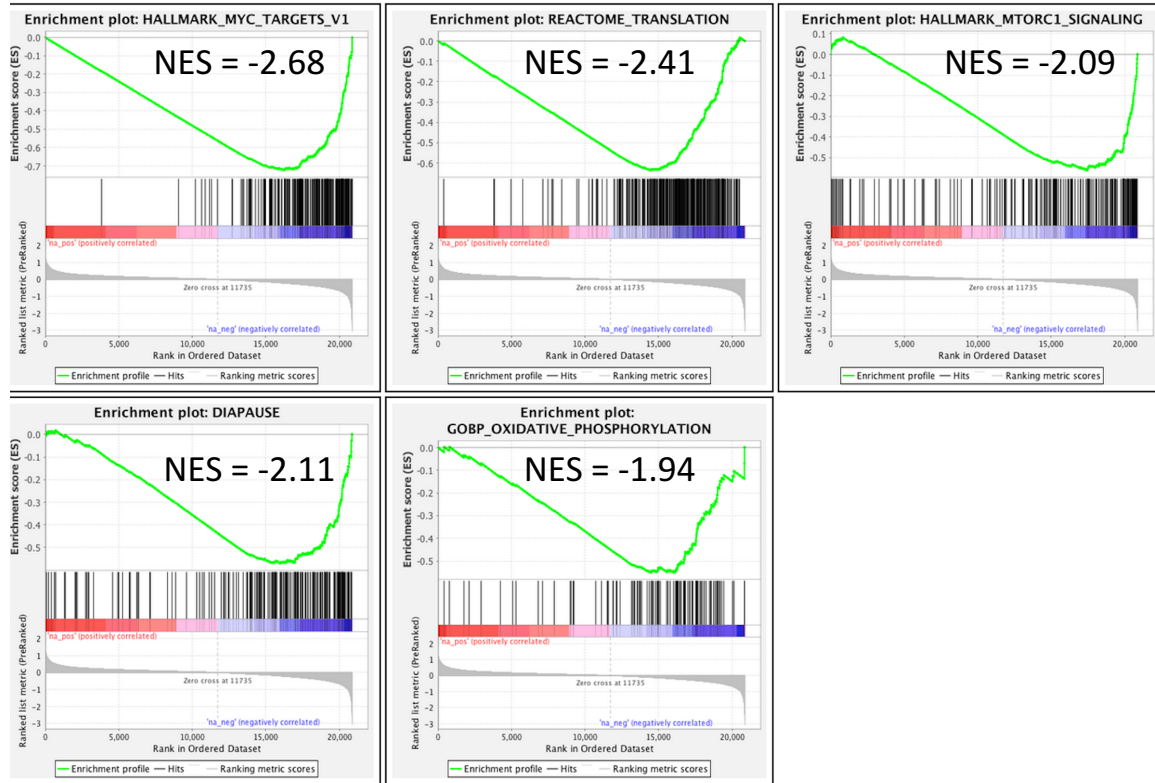
B

| Name	gene.index	RP/Rsum	FC:(Resistant/Ctrl)	pfp	p.value
SELM	17508	116.8	2.17	0.016	0.00000076
CRYAB	10602	134	2.3	0.014	0.0000013
BRCA1	7273	218.2	2.03	0.037	0.0000089
DEPTOR	14054	247.8	1.79	0.05	0.000015
SOX2	12195	255.5	1.68	0.048	0.000016
TMEM45A	14482	257.4	2.01	0.044	0.000017
GDA	4559	260.6	2.15	0.041	0.000018
CEACAM6	6751	261.8	2.1	0.037	0.000018
PTPRD	8135	285.7	2.16	0.047	0.000025

C

Supplementary Fig. S6: A: Gene set enrichment analysis (GSEA) depicting transcriptional changes in CBP-treated residual PDXs vs mock-treated PDXs (O3312, O1047, O5588). These five signatures are hallmarks of the Diapause program (Dhimolea et al., Cancer Cell 39:240-256 (2021)). The graphs show the enrichment score. The plot represent the enrichment score of the genes included in the tested signature and relative expression of each individual gene appears as a black line. In all cases FDR <0.001. NES are indicated on each graph. Done with the GSEA software (Subramanian (2005) with pre-rank option. **B:** Overexpressed genes in acquired-resistant PDXs vs control PDXs. PDXs with acquired-resistance *in vivo* from models O3312 and O8378 were compared to corresponding naive PDXs. Rankprod pfp<0.05. **C:** Scheme of comparisons done for the transcriptomic analysis to identify overexpressed genes in common between Residual and Resistant tumors.
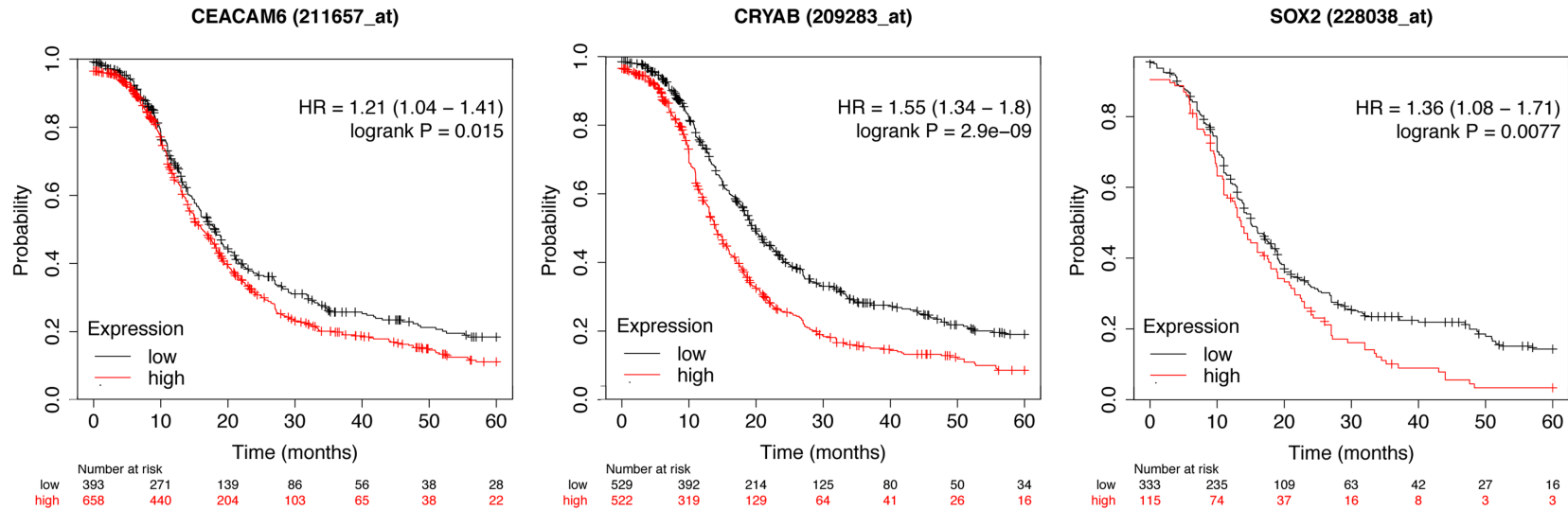
Supplementary Fig. S7: HGOC expressing high levels of CEACAM6 or CRYAB or SOX2 recur earlier than those with low levels. Tumors were stratified according to the expression level of either *CEACAM6 or CRYAB* or *SOX2 and* Kaplan-Meier progression free survival graphs generated with the Kmplot tool on line (https://kmplot.com/analysis/, access in mars 2021) using all serous HGOC.
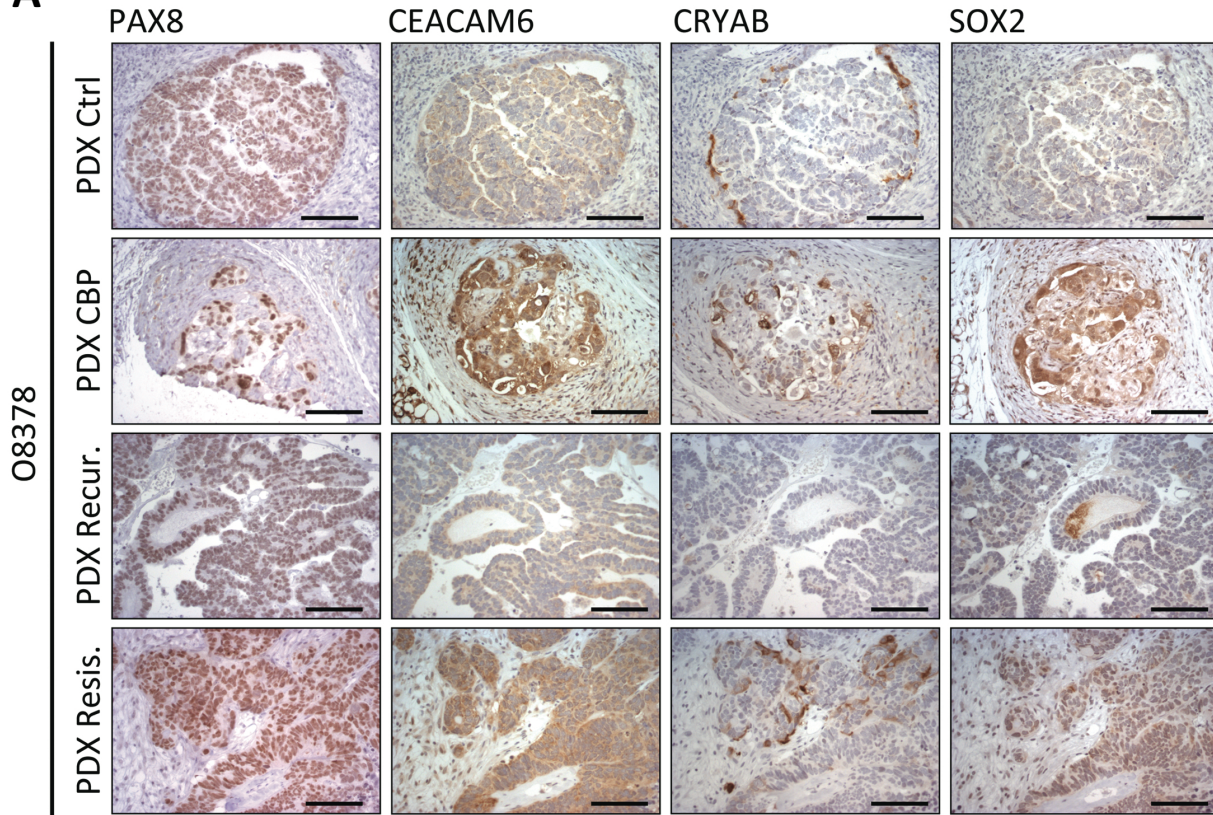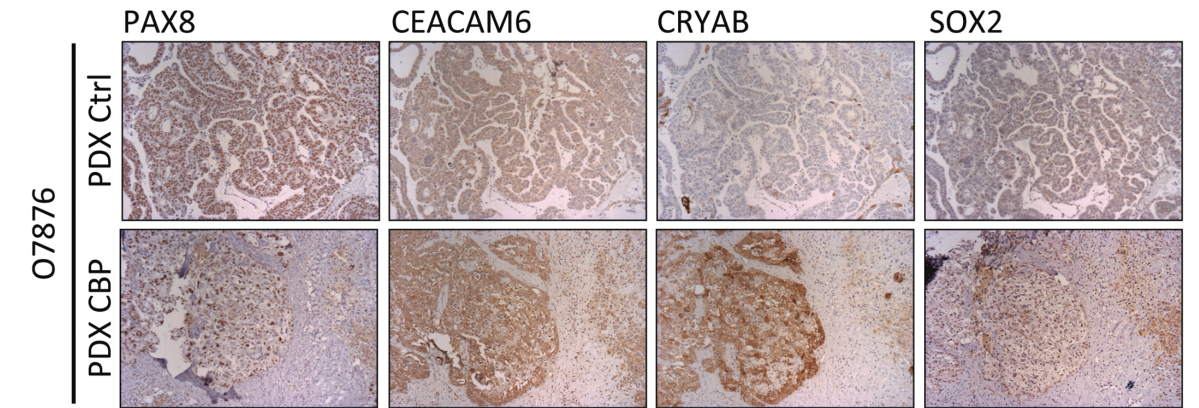
Supplementary Fig. S8: PAX8, CEACAM6, CRYAB and SOX2 representative IHC staining. Immunostained proteins are indicated on top. Bars corresponds to 100 microns. **A:** histological sections of O8378 CBP-sensitive PDX. **B:** section of CBP-senstive O7876 PDX. Signification of the legends are as follows; PDX ctrl = mock-treated, PDX CBP = CBP-treated, PDX Recur. = PDX recurrence, PDX resis = PDX with acquired resistance.
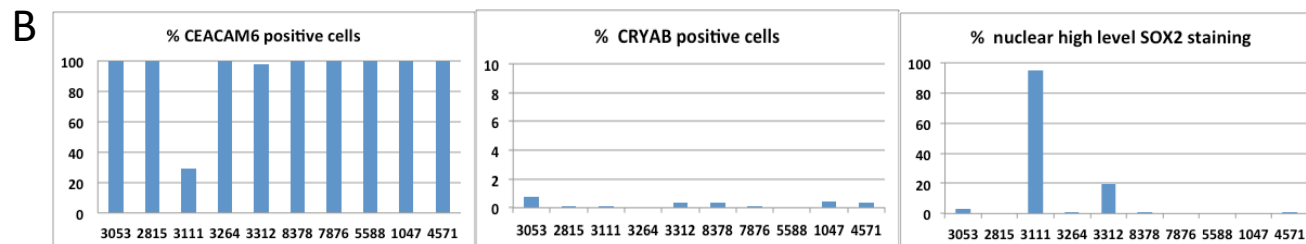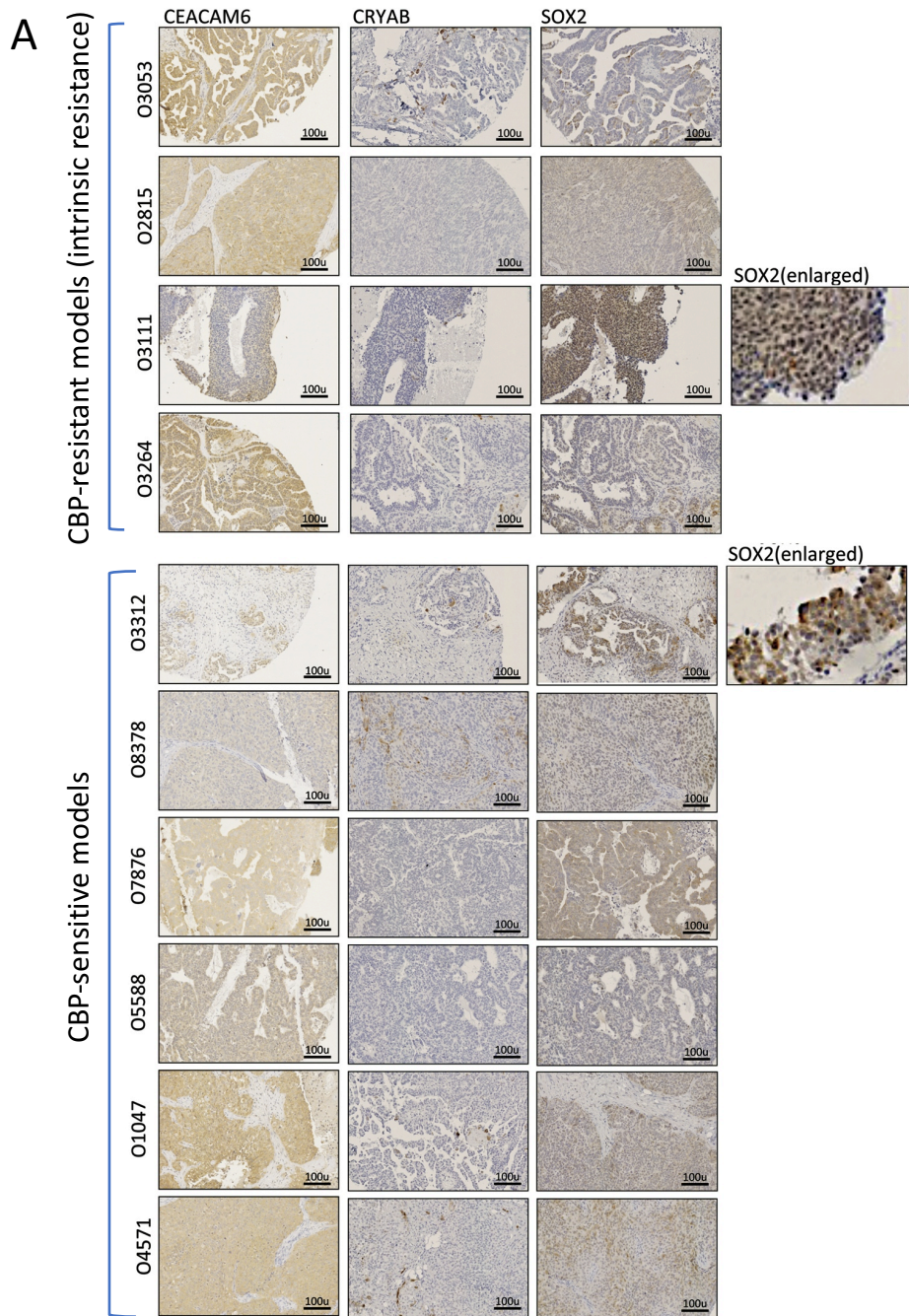
Supplementary Fig. S9: A: IHC staining of PAX8, CEACAM6, CRYAB and SOX2 in the 10 PDX models on a TMA. **B:** Corresponding quantifications of positive cells. For CEACAM6, a weak staining was observed in most of cells except for O3111 which presented a weaker staining. CRYAB staining was found in less than 1% for all PDXs. Strong nuclear SOX2 staining was detectable in most cells of O3111 (CBP-Resistant). About 20 % of cells of O3312 (CBP-Sens) displays a strong nuclear SOX2 staining whenever other PDXs were negative (<1%).
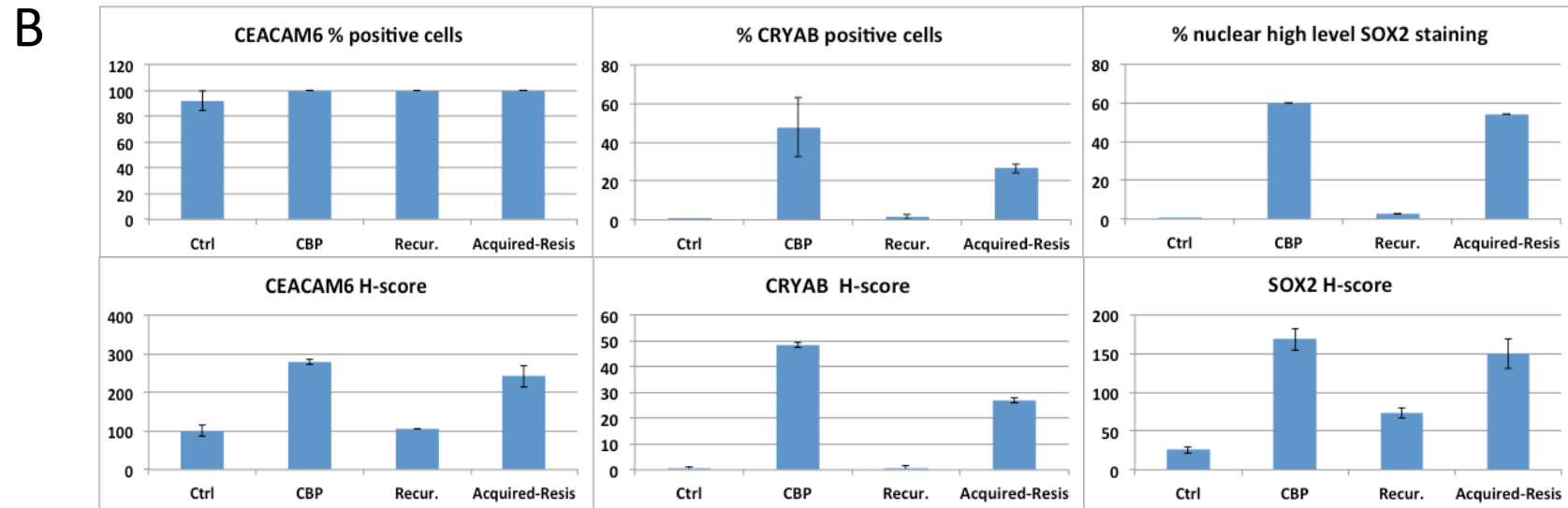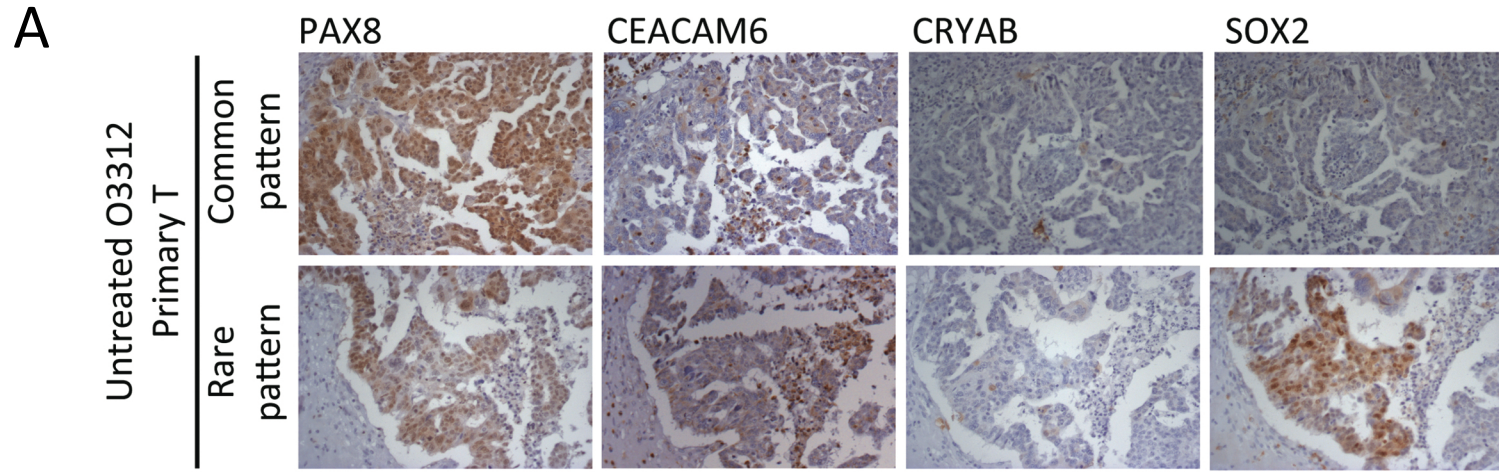
Supplementary Fig. S10: A : PAX8, CEACAM6, CRYAB, SOX2 immunostaining in tissue sections from the patient tumor from which O3312 was derived (Primary T). The most common staining pattern was CEACAM6 weak/CRYAB null/SOX2 null. Some rare areas showed cell clusters with nuclear SOX2 staining. **B** : Quantification of CEACAM6 or CRYAB or SOX2 staining in O3312 PDXS using the QuPath software. Percentage of positive cells and H-score are presented.